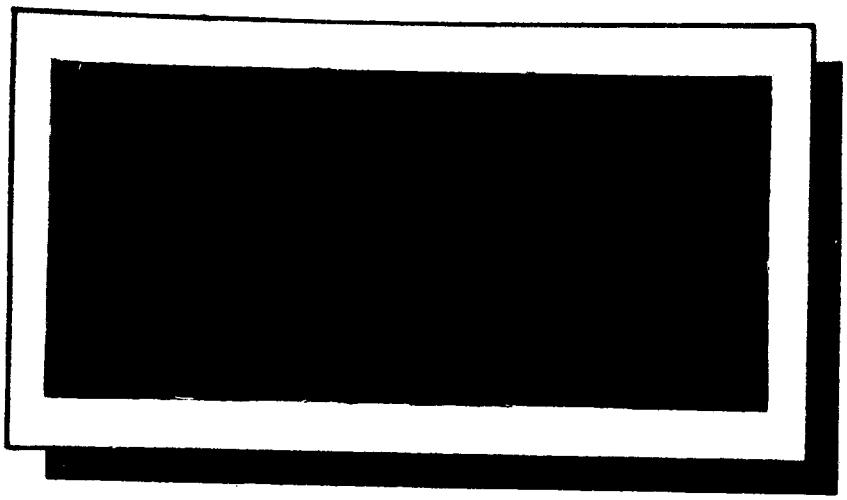

CENTER FOR SPACE RESEARCH

MASSACHUSETTS INSTITUTE OF TECHNOLOGY

Cambridge Mass 2

3 CONTINUUM ELECTROMECHANICS GROUP

Electromechanical Co-Streaming

and Counter-streaming Instabilities 6

6 by Frederick D. Ketterer 9

9 August 1966 6 29B CSR-TR-66-15 26 NSG-368 - 2 1 N C Y

C 4

END

ELECTROMECHANICAL CO-STREAMING AND COUNTER-STREAMING INSTABILITIES

Frederick D. Ketterer

Massachusetts Institute of Technology
Department of Electrical Engineering

Abstract

The dynamics of two highly conducting, finite length streams in relative motion, coupled by a transverse electric or longitudinal magnetic field are examined in detail. The systems may be mathematically described by two second order coupled hyperbolic partial differential equations. Four classes of flow exist: (1) subcapillary (2) supercapillary co-streaming (3) supercapillary counter-streaming and (4) subcapillary-supercapillary flow. The first three are considered in the present paper. The behavior of the infinitely long system is examined from the dispersion relation and the Bers-Briggs stability criterion. The eigenvalue problem is formulated for class (1) and (3) flows (no eigenvalues exist for class (2) flow) and the complex eigenfrequencies computed. Electrohydrodynamic experiments on these systems are described and compared with the theory. Physical explanations are given for the observed instabilities.

I. Introduction

Kelvin-Helmholtz instability arises when adjacent layers of fluid are in relative motion. A simple explanation of this instability may be given on the basis of convected momentum (Bernouilli instability)[1], but this leads to a naive picture of real fluid mechanics, since it assumes that the layers may slide freely over each other. Chandrasekhar[2] offers an introduction to the classical Kelvin-Helmholtz instability. If a realistic model including viscosity is postulated, the problem becomes quite complicated, and only recently have numerical solutions been obtained for specific models.[3]

Kelvin-Helmholtz instability is not restricted to classical fluids. Special cases of the hydromagnetic version have been considered by Fejer,[4] Michael,[5] Northrop,[6] Alterman,[7] and Sen.[8] The only work done on the electrohydrodynamic Kelvin-Helmholtz instability is by Lyon,[9] who derived the dispersion relation for two streaming inviscid dielectric fluids (in contact) stressed by an electric field. Considerable attention has been given recently to streaming instabilities in plasmas, both gaseous[10,11] and solid state.[12] Devices employing electron beam injections into a plasma as a possible scheme for thermonuclear heating are being studied.[13] Some experiments involving counter-streaming electron beams, complicated by the presence of a background plasma, are as yet unexplained, and are currently the subject of research.[14,15]

The continuum electromechanical situations considered here can be modeled by a relatively simple theory which provides good agreement with experiment. The electrohydrodynamic model consists of two highly conducting streams in relative motion and coupled by an electric field. Electrical coupling eliminates the difficulty encountered in modeling two real fluids in physical contact. An analogous situation exists in magnetohydrodynamics, in which the electric field is replaced by a magnetic field. Here the coupling is produced by a magnetic field trapped between two perfectly conducting fluid streams. These situations compliment each other and both will be considered in the same context.

It should be noted that the implications of the results presented here are not restricted simply to electromechanical systems. Indeed, analogous situations exist in two-stream electron beam interactions, and in solid state plasmas. Waves are considered to be propagating in the direction of streaming (the longitudinal direction). In general, the imposition of transverse boundaries produces an infinite set of modes of propagation. To solve for these modes, with both longitudinal and transverse boundaries imposed, is an immense problem. The conventional technique is to assume that wavelengths of interest (in the longitudinal direction) are short compared to the length of the system so that the effect of longitudinal boundaries may be ignored. Quite often, and in all the cases considered here, the long waves are the most significant and play a more important role in determining the dynamics than higher

order transverse modes. For this reason, the effects of longitudinal boundaries will be carefully considered, while at the same time including the effect of only the principle transverse modes. It is possible then to provide a complete picture of the system dynamics. The correct model for the longitudinal boundary conditions can be unambigously specified. This is not possible in general, since boundary conditions consistent with causality may not be clearly defined.

It should be pointed out that coupled mode theory,[16] used extensively in complex systems with interacting waves, particularly in electron beam devices, is not particularly useful for electric field coupled systems since the uncoupled modes have complex wavenumbers.

II Problem Description

The mathematical model consists of two highly conducting fluid streams in relative motion, stressed by an electric or magnetic field (Figure 1). The assumed planar geometry simplifies the mathematics considerably and it will be shown that experimental results obtained using circular jets are in quantitative agreement with this model if the coupling coefficients in the equations of motion are experimentally determined. Attention will be restricted to a study of the kink modes ($m = 1$) of the jets. Measurements by Crowley[17] on the dynamics of a single jet stressed by a transverse electric field support the validity of the model.

The equations of motion for the streams may be written[18]

$$\left(\frac{\partial}{\partial t} + V_{o_1}\frac{\partial}{\partial x}\right)^2 \xi_1 - V_{t_1}^2 \frac{\partial^2 \xi_1}{\partial x^2} - \frac{\eta}{2}\omega_{e_1}^2 \xi_1 = -\frac{1}{2}\omega_{e_1}^2 \xi_2$$

$$\left(\frac{\partial}{\partial t} + V_{o_2}\frac{\partial}{\partial x}\right)^2 \xi_2 - V_{t_2}^2 \frac{\partial^2 \xi_2}{\partial x^2} - \frac{\eta}{2}\omega_{e_2}^2 \xi_2 = -\frac{1}{2}\omega_{e_2}^2 \xi_1 \qquad (1)$$

where

$$V_{t_{1,2}} = \sqrt{\frac{2T_{1,2}}{\rho_{1,2}\Delta}} \qquad \omega_{e_{1,2}} = \sqrt{\frac{2\epsilon_o E_o^2}{(2a-\Delta)\rho_{1,2}\Delta}} \qquad \eta = \frac{b+a-\frac{3\Delta}{2}}{b-a-\Delta/2}$$

$$\omega_{h_{1,2}} = \sqrt{\frac{2\mu_o H_o^2}{(2a-\Delta)\rho_{1,2}\Delta}}$$

In the above equations, T is the surface tension, ρ is the fluid density, ξ the transverse displacement of the streams from equilibrium, V_o the equilibrium stream velocity, E_o and H_o the equilibrium electric and magnetic fields respectively. The equation for magnetic coupling is obtained from Equation (1) by replacing ω_e^2 by $-\omega_h^2$.[19]

The following assumptions have been made in the derivation of Equation (1):

(a) linear theory

(b) no viscous or resistive effects

(c) long wave model ($\lambda >> |b-a|$ or a)

(d) all equilibrium quantities are constants.

(e) planar thin streams, $\Delta << a$

Equation (1) with $\omega_e = 0$ is simply the equation of a vibrating string with convective velocity V_o. The third term in Equation (1), the self-coupling term, represents the net traction of electrical origin acting on the stream caused by a deflection of that stream. Similarly, the last term, the mutual coupling term, is the net electrical traction caused by the deflection of the other stream. The quantities ω_e and ω_h both have physical significance. Consider for the moment three parallel equally spaced conducting plates with the center plate free to move, and equal electric fields applied above and below the plate. Then an upward displacement concentrates the E field lines above the plate, weakens them below, with the result that the unbalanced electric stress is destabilizing. The parameter ω_e is the growth rate of instability of the plate. The electric field in effect plays the role of a distributed negative spring. For the single stream, if the flow velocity $V_o < V_t$ the behavior is an absolute static ($\omega_r = 0$) instability, whereas for $V_o > V_t$, it is a convective instability.[19]

For magnetic field coupling, an upward displacement compresses the field lines above, expands them below the body; the resultant magnetic pressure is stabilizing and ω_h is the frequency of oscillation

in the field. A single subcapillary stream ($V_o < V_t$) exhibits evanescence below a cutoff frequency, while the supercapillary stream ($V_o > V_t$) exhibits only propagating waves.

One might expect this antiduality to carry over into two-stream systems as well. This is only partially true, however, and it will be seen that those instabilities which are Kelvin-Helmholtz in character exist whichever type of field is used.

Since Equation (1) consists of two coupled wave equations, there are four characteristic velocities of propagation,[20] namely, $V_{o_{1,2}} \pm V_{t_{1,2}}$. This means there are four distinct flow configurations possible. In addition, it is easy to show by means of the method of characteristics that the longitudinal boundary conditions consistent with causality are uniquely specified once the characteristic lines are determined. These are summarized below and Classes I - III will be discussed in the following sections. Work concerning the Class IV system will be reported.

Class	Flow Conditions	No. Boundary Conditions			
		Stream 1		Stream 2	
		x = 0	x = L	x = 0	x = L
I	$\lvert V_{o_1}\rvert < V_{t_1}$ $\lvert V_{o_2}\rvert < V_{t_2}$	1	1	1	1
II	$V_{o_1} > V_{t_1}$, $V_{o_2} > V_{t_2}$	2	0	2	0
III	$V_{o_1} > V_{t_1}$, $V_{o_2} < -V_{t_2}$	2	0	0	2
IV	$\lvert V_{o_1}\rvert > V_{t_1}$ $\lvert V_{o_2}\rvert < V_{t_2}$	2	0	1	1

The dispersion relation for the system is obtained directly from Equation (1) by assuming solutions of the form $e^{j(\omega t-kx)}$ for $\xi_{1,2}$.

$$\left[(\omega-V_{o_1}k)^2 - V_{t_1}{}^2k^2 + \frac{\eta}{2}\omega_{e_1}{}^2\right]\left[(\omega-V_{o_2}k)^2 - V_{t_2}{}^2k^2 + \frac{\eta}{2}\omega_{e_2}{}^2\right] - \frac{1}{4}\omega_{e_1}{}^2\omega_{e_2}{}^2 = 0 \tag{2}$$

and ω and k are complex, $\omega = \omega_r + j\omega_i$ and $k = k_r + jk_i$.

III Class I Coupled Elastic Continua

If both streams have subcapillary flow velocity, the behavior is basically that of two field coupled elastic membranes; the effect of flow velocity merely changes the details. For convenience, let $V_{t_1} = V_{t_2} = V_t$ and $\omega_{e_1} = \omega_{e_2} = \omega_e$. The dispersion relation(Equation (2))is plotted in Figure 2, where ω and k have been scaled to $\omega_{e,h}$ and $\frac{\omega_{e,h}}{V_t}$ respectively. From Equation (2) it is evident that η is replaced by $-\eta$ for magnetic coupling. Figure 2(a) and (b) respectively show electric field coupling with the mutual coupling between the streams excluded (single stream interactions) and with the mutual interaction included. The same is true in Figure 2(c) and (d) for magnetic coupling. In Figure 2(b) it is seen that first two waves, then all four waves become unstable. (complex ω) as k is reduced, the growth rate increasing as the wave tends to zero. It is easily shown from the Bers-Briggs[21,22] criterion that these instabilities are absolute and static ($\omega_r = 0$), as shown in Figure 3. The method of Bers and Briggs provides a criterion in distinguishing whether a wave is propagating, evanescent, convectively unstable, or absolutely unstable. The method consists in plotting the complex k values of the dispersion relation for fixed ω_r as ω_i is increased from $-\infty$ to zero.

For example, for k's originating below the k_r axis, if a k locus remains below the k_r axis when $\omega_i \rightarrow 0$, it represents a decaying or evanscent wave; if it lies on the axis, it is a purely propagating wave to the right, and if it crosses the axis it becomes an amplifying wave or convective instability. For k's originating above the k_r axis, a similar statement is valid. If, however, two k loci join, one from above, one from below the k_r axis and split to form a saddle point as $\omega_i \rightarrow 0$, this signifies an absolute instability; the value of ω_s (saddle point frequency) gives the frequency and growth rate, the value of k_s the spatial dependence. Finally, ω_r is varied to obtain the wave properties for all frequencies. Figure 3 exhibits two saddle points, which is reasonable since each stream separately exhibits a single saddle point. For magnetic coupling (Figure 2(c)), we observe that each stream exhibits evanescence, which is also exhibited by the coupled system.

While the Class I regime is not particularly interesting from the point of view of introducing new phenomena, it provides a means of calibrating an experiment to test the other flow regimes. Consider the special case $V_{o_1} = V_{o_2} = 0$. The motion can be seen to be composed of two symmetry modes, a symmetric mode, $\xi_1(x,t) = -\xi_2(x,t)$, and an anti-symmetric mode, $\xi_1(x,t) = \xi_2(x,t)$, or the S and A modes respectively. The dispersion equation for electric field coupling reduces simply to

$$\omega^2 - V_t^2 k^2 + \omega_e^2 \frac{\eta \pm 1}{2} = 0 \quad \begin{pmatrix} S \\ A \end{pmatrix} \tag{3}$$

Two saddle points exist,

$$\omega_s = -j\omega_e\sqrt{\frac{\eta \pm 1}{2}} \quad \begin{pmatrix} S \\ A \end{pmatrix} \tag{4}$$

$$k_s = 0$$

If we now consider the system to be of finite length and impose the boundary conditions $\hat{\xi}_{1,2}(0) = \hat{\xi}_{1,2}(L) = 0$ where $\xi_{1,2}(x,t) = \hat{\xi}_{1,2}(x)e^{j\omega t}$, we obtain the eigenvalue equation

$$\omega^2 + \omega_e^2 \frac{\eta \pm 1}{2} = \left(\frac{n\pi}{L}\right)^2 V_t^2 \quad \begin{pmatrix} S \\ A \end{pmatrix} \tag{5}$$

From (5) the resonant frequency is simply $\frac{n\pi V_t}{L}$ at zero electric field and decreases to zero as the electric field is raised to the critical value given by

$$\omega_{e_{crit.}} = \frac{n\pi V_t}{L} \Big/ \sqrt{\frac{\eta \pm 1}{2}} \tag{6}$$

We observe that the fundamental mode is the first to go unstable and that the symmetric mode becomes unstable at a lower critical field than the antisymmetric mode. Further, the maximum growth rate of instability is obtained as $L \to \infty$ and is given by the saddle point above. This is as expected since it means that the boundaries have a stabilizing influence.

An Experiment

Stable planar fluid streams are quite difficult to produce experimentally.[23] Instead, cylindrical fluid streams will be used. However, the analysis for this system is extremely complicated. The assumption is made here that the experimental behavior can be predicted

by a planar model if the system parameters are determined experimentally. A fluid jet of zero velocity can be simulated quite well by a closely wound weak spring (having approximately the same linear density although a considerably higher tension than that due to the surface tension of liquid jets). This experiment will serve both as verification of the model and as calibration of the apparatus for later experiments.

Two matched springs 1/8" dia and 80 cm length were stretched to the same tension between parallel rigid supports in the horizontal plane to eliminate gravitational effects. A rigid rod was placed parallel to each spring to provide electrical equilibrium. By carefully adjusting the outer plates, it was possible to establish force equilibrium using a single DC voltage source. From Equation (5) we observe that a plot of frequency squared vs. voltage squared should yield two straight lines of negative slope. The resonant frequency was measured by superimposing a small AC voltage on the previously grounded plate and varying the frequency for maximum spring deflection. The results in Figure 4 follow the predicted behavior and provide the determination of ω_e and η. At high voltage the equilibrium positions of the springs were displaced, which accounts for the deviation of the curve from a straight line.

IV Class II Coupled Costreaming Jets

If the two streams have flow velocities $V_o > V_t$, then the dynamics are quite different. In this case, all waves propagate downstream and since

all boundary conditions are imposed at the same point in space, there are no eigenfrequencies. The absolute instabilities for subcapillary flow and electric field coupling discussed previously now become convective instabilities, as seen in the dispersion curves of Figure 5, and verified by the Bers-Briggs criterion. Since there are no absolute instabilities, the system may be excited in the sinusoidal steady state. If the flow velocities are equal, the system possesses symmetry modes as in the previous case. From the dispersion equation, the wave-number becomes

$$k = \frac{\omega V_o}{V_o^2 - V_t^2} \pm \beta$$

where

$$\beta_{\substack{S \\ A}} = \frac{\sqrt{\omega^2 V_t^2 - (V_o^2 - V_t^2)\omega_e^2 \frac{\eta \pm 1}{2}}}{V_o^2 - V_t^2} \quad \binom{S}{A} \tag{7}$$

Thus the system has a cutoff frequency for spatial growth given by

$$\omega_{cutoff} = \omega_e \sqrt{(V_o^2 - V_t^2)\frac{\eta \pm 1}{2}} \quad \binom{S}{A}$$

below which the waves are amplifying. The symmetric mode exhibits the larger spatial growth, and the growth rate becomes maximum as $\omega \rightarrow 0$. These effects have been qualitatively verified experimentally.

The dispersion curves for magnetic coupling are shown in Figure 6. It is seen that for flow velocities approximately equal the system behaves

essentially as if the jets were mutually uncoupled and exhibits only propagating waves. However, if the streams have sufficiently different flow velocities, then the fast wave on one stream couples to the slow wave on the other stream to produce an amplifying wave. This situation also exists in electron beams; in fact, the equation for longitudinal oscillations in an electron beam can be obtained from the magnetic coupled equations by letting $V_t \rightarrow 0$ and $\eta \rightarrow 1$.

V Class III Counterstreaming Jets

The dynamics of two coupled oppositely directed supercapillary streams is quite different from the cases considered so far. In this case, waves can propagate only downstream on each jet, but since they are oppositely directed an internal feedback mechanism is available which potentially at least could provide instability. Typical dispersion curves are shown in Figure 7. For electric field coupling, there appears to be little coupling except at the origin where the curves join. While the system is evidently unstable, it is not clear what kind of instability is present. The Bers-Briggs stability plots are shown in Figure 8. From curve 1 of Figure 8a, the conditions for a saddle point are present, with ω_s being purely imaginary indicating a static instability. The spatial dependence is exponential. In addition there is a mild overstability in the neighborhood of the loci of curves 3 and 4.

The dispersion relation for magnetically coupled counter-streaming jets is shown in Figure 7c and d. This system also exhibits instability,

and from curves 1 and 2 of Figure 8b, it is clear that it is an overstability. The spatial character of the instability is essentially wave-like, contrasting the electric field coupled case.

If we now consider the important case $V_{o_1} = -V_{o_2} = V_o$, a considerable simplification of the mathematics results. The dispersion relation simplifies to

$$(V_o^2 - V_t^2)^2 k^4 + k^2\left[\omega_e^2 \eta (V_o^2 - V_t^2) - 2\omega^2(V_o^2 + V_t^2)\right] + \omega^4 + \omega^2\omega_e^2\eta + \omega_e^4 \frac{\eta^2-1}{4} = 0 \tag{8}$$

which is biquadratic in both k and ω, a consequence of the two flow speeds being equal. If we examine (8) for possible saddle points, we seek the frequencies with negative, imaginary part which will result in double roots in k. Since it is of the form $Ak^4 + Bk^2 + C = 0$ the possibilities are: (a) $C = 0$ which means $k = 0$ and $\omega_s = -j\omega_e\sqrt{\frac{\eta \pm 1}{2}}$. Comparison with Figure 8a shows that the saddle point is $k_s = 0$ and $\omega_s = -j\omega_e\sqrt{\frac{\eta + 1}{2}}$ (b) $B^2 - 4AC = 0$, which means $k = \pm \frac{-B}{2A}$, but the corresponding frequencies are stable.

This means that as the velocity of the jets are made equal in magnitude, the overstability observed in Figure 8a disappears and the static instability is not appreciably changed.

For magnetic field coupling, condition (b) above produces the saddle point, given by

$$\omega_s = \frac{-j\sqrt{(V_o^2-V_t^2)\eta}\,\omega_h}{2V_t}\sqrt{1-\sqrt{1-V_t^2/V_o^2}} \approx \frac{-jV_t\omega_h}{V_o} \quad \text{for } \frac{V_t^2}{V_o^2} \ll 1$$

$$k_s = \pm\,\omega_h\sqrt{\frac{\eta}{2(V_o^2-V_t^2)}\left[1-\left[1-\sqrt{1-\frac{V_t^2}{\eta^2 V_o^2}}\right]\right]\frac{(V_o^2-V_t^2)}{2V_t^2}} \sim \frac{\omega_h}{V_o}\sqrt{\frac{\eta}{2}\left(1-\frac{1}{4\eta^2}\right)} \qquad (9)$$

The effect in Figure 8b of making the velocities of equal magnitude is to shift the saddle point frequency to the $j\omega$ axis (static instability) and to make the wavelength real.

If we now compare the electric field coupled and magnetic field coupled models, two facts become evident. First, from the saddle point frequencies, the electric field coupled system is more unstable than the magnetic field system (by a factor of 4 for $\eta = 2$ and $V_o/V_t = 3$). Second, both systems are statically (absolutely) unstable, even though neither system is absolutely unstable without the mutual coupling. As stated previously, the electric field self coupling term is destablizing while for magnetic coupling it is stabilizing.

The conclusion is that the instability is caused by the mutual interaction of the two counter-streaming supercapillary streams and is therefore Kelvin-Helmholtz in character, contrasting the previously considered instabilities which were Rayleigh-Taylor in nature. To investigate this further, if the stability is re-examined with both the self coupling terms and the surface tension eliminated, both systems

are found to be statically unstable with the same growth rate. It is physically reasonable that this should be so since whether the streams pull on each other (electric field coupling) or push on each other (magnetic field coupling) is immaterial.

The Eigenvalue Problem

Since boundary conditions must be imposed at two different points in space, the system possesses eigenvalues. This system is unusual, however, in that each stream is free to move at its downstream end. Furthermore, two counter-streaming jets is an example of a system which does not possess eigenvalues in the uncoupled state.

To determine the natural modes, each jet will be assumed to enter the interaction region unexcited. The boundary conditions are:

$$\xi_1(-L\ t) = \frac{\partial\ \xi_1}{\partial x}(-L\ t) = 0$$
$$\xi_2(L\ t) = \frac{\partial \xi_2}{\partial x}(+L\ t) = 0 \qquad (10)$$

where L = half length of the jets.

The problem can be considerably simplified by again taking advantage of the symmetry which exists if the flow velocities are of equal magnitude. It can be seen that both the equations of motion and the boundary conditions are satisfied if the symmetric and antisymmetric modes are expressed by $\xi_1(x_1 t) = \mp \xi_2(-x_1 t)$ respectively; i.e., the symmetry is now about the origin as shown in Figure 9 instead of the longitudinal axis as before.

From Equation (1) we may assume a solution $\xi(x,t) = \hat{\xi}(x)e^{j\omega t}$ so that $\hat{\xi}_1(x) = \sum_{i=1}^{4} B_i e^{-jk_i x}$ where the k's are determined from the biquadratic dispersion equation. The solution for jet 2 is then given by

$$\hat{\xi}_2(x) = \frac{2}{\omega_e^2}\left[(j\omega + V_o\frac{d}{dx})^2 - V_t^2\frac{d^2}{dx^2} - \frac{\eta\omega_e^2}{2}\right]\hat{\xi}_1(x)$$

This may be written in simpler form as a linear combination of odd and even functions of x.

$$\hat{\xi}_1(x) = A_1\delta_{e_1}(x) + A_2\delta_{o_1}(x) + A_3\delta_{e_2}(x) + A_4\delta_{o_2}(x)$$

$$\hat{\xi}_2(x) = \frac{2}{\omega_e^2}\left[\omega^2 - (V_o^2 - V_t^2)\frac{d^2}{dx^2} + \frac{\eta}{2}\omega_e^2\right]\hat{\xi}_1(x) - \frac{2}{\omega_e^2}(2j\omega V_o)\frac{d\hat{\xi}_1(x)}{dx} \tag{11}$$

where

$$\delta_{e_{1,2}}(x) = \cos\beta_{1,2}x\cosh\alpha_{1,2}x - j\sin\beta_{1,2}x\sinh\alpha_{1,2}x$$

$$\delta_{o_{1,2}}(x) = \cos\beta_{1,2}x\sinh\alpha_{1,2}x - j\sin\beta_{1,2}x\cosh\alpha_{1,2}x \tag{12}$$

and

$$k_{1,2} = \beta_{1,2} + j\alpha_{1,2}$$

Applying the symmetry conditions we get

$$\hat{\xi}_1(x) = A_1\left[\delta_{e_1}(x) + \Gamma_1\delta_{o1}(x)\right] + A_3\left[\delta_{e_2}(x) + \Gamma_2\delta_{o2}(x)\right]$$

where $\Gamma_{1,2} = \dfrac{\omega^2 + k_{1,2}^2(V_o^2 - V_t^2) + \omega_e^2\frac{\eta \pm 1}{2}}{2\omega V_o k_{1,2}}$ $\quad (^{S}_{A})$ (13)

Substituting the boundary conditions into Equation (13) yields the following eigenvalue equation.

$$k_1\left[\Gamma_1\delta_{e1}(L)-\delta_{o1}(L)\right]\left[\delta_{e2}(L)-\Gamma_2\delta_{o2}(L)\right]-k_2\left[\delta_{e1}(L)-\Gamma_1\delta_{o1}(L)\right]\left[\Gamma_2\delta_{e2}(L)-\delta_{o2}(L)\right]=0 \tag{14}$$

This equation, combined with the dispersion relation, yields an expression $\Delta(\omega, V_o, V_t, \omega_e, \eta, L) = 0$ which in principle can be solved to obtain the complex eigenfrequencies as a function of the parameters of the system. The important parameters of the system are V_o, ω_e, and L; by suitably scaling ω to ω_e and L to V_o/ω_e the number of parameters may be reduced and the eigenvalue equation becomes, $\Delta(\omega/\omega_e, V_t/V_o, \eta, L\omega_e/V_o) = 0$. The effects of V_t/V_o and η are small, so that essentially $\Delta(\omega/\omega_e, L\omega_e/V_o) = 0$ is the functional dependence desired.

The resulting eigenfrequency versus normalized length curves for the lowest three symmetric and antisymmetric modes are shown in Figure 10. For small field or short length, all modes represent decay, the normalized decay rate $\longrightarrow \infty$ as the length $\longrightarrow 0$. The effects of the boundaries are strongly stabilizing. For a very long system, the modes which are unstable approach two asymptotic values, the more unstable of which is the saddle point predicted by the Bers-Briggs criterion for the infinite length system. Thus the asymptotic behavior at large and small values of $L\omega_e/V_o$ are physically expected.

However, there are several facts which cannot be predicted from the dispersion relation alone. The lowest S and A mode eigenfrequencies are purely imaginary; the A mode remains a decay mode, while the S mode

becomes unstable as $\frac{L\omega_e}{V_o}$ is increased and finally approaches the saddle point frequency. This is the most unstable mode of the system. All modes above the fundamental are dynamic ($\omega_i \neq 0$), until a critical value of $L\omega_e/V_o$ is reached for each mode when the modes become purely static growth or decay. Thus modes A2, S3, A4, etc., are particularly interesting since they represent overstabilities. In an experiment, however, these modes would be virtually impossible to see because of the overriding static instability of the fundamental symmetric mode.

At the point of impending instability $\omega = 0$, and the constraint on the parameter values may be calculated from Eq.(14) and the dispersion relation. Thus,

$$(V_o^2 - V_t^2)k^4 + k^2 \omega_e^2 (V_o^2 - V_t^2) + \omega_e^4 \frac{\eta^2 - 1}{4} = 0$$

Solving for k, $\quad k = \pm j\omega_e \sqrt{\frac{\eta \pm 1}{2(V_o^2 - V_t^2)}}$

From Equation (13) Γ_1 and Γ_2 become indeterminate at $\omega = 0$, but in the limit $\omega_i \to 0$, Γ_1 and Γ_2 are of order $\frac{1}{\omega_i}$ and ω_i respectively so that $\Gamma_2 \to 0$. This simplification yields for the condition of impending instability

$$\tanh\left[\frac{\omega_e L}{\sqrt{V_o^2 - V_t^2}}\sqrt{\frac{\eta+1}{2}}\right] \tanh\left[\frac{\omega_e L}{\sqrt{V_o^2 - V_t^2}}\sqrt{\frac{\eta-1}{2}}\right] = \sqrt{\frac{\eta-1}{\eta+1}} \qquad (15)$$

Equation 15 is plotted in Figure 11 as $\frac{\omega_e L}{\sqrt{V_o^2 - V_t^2}}$ vs. a/b. (Since Δ can be absorbed in a and b, Δ is taken to be zero here.) As can be seen the point of instability is not strongly affected by transverse geometry, except when the external plates are placed very close to the fluid streams, when the required electric field for instability tends to zero. This is physically reasonable, since a small displacement on the stream will produce a large change in the electric traction.

The eigenfunctions for the point of impending instability are easily calculated. From Equation (14), setting $\omega = 0$ and applying the boundary conditions for the symmetric mode $\hat{\xi}(-L) = \frac{\partial \hat{\xi}(-L)}{\partial x} = 0$

$$\hat{\xi}_{1,2}(x) = \xi_o \left[\frac{\sinh \alpha_1 x}{\sinh \alpha_1 L} \pm \frac{\cosh \alpha_2 x}{\cosh \alpha_2 L} \right] \tag{16}$$

where

$$\alpha_{1,2} = \frac{\omega_e}{\sqrt{V_o^2 - V_t^2}} \sqrt{\frac{\eta \pm 1}{2}}$$

The open endedness of the jets is clearly evident in Equation (16) and contrasts the displacement of the fundamental mode of the two-spring system. The plot is essentially that shown in Figure 12, where the eigenfunctions for $\frac{L\omega_e}{V_o} = 3$ for the lowest three symmetric and antisymmetric modes are plotted. The dynamical behavior is evident from the display of the trajectories at three successive instants of normalized time.

The stability and symmetry are apparent. Since the eigenfrequency for the fundamental modes is imaginary, the trajectories exhibit no phase shift for increasing time. The higher modes, on the other hand, all exhibit propagating behavior as well as growth or decay in time.

Numerical Computation

The solution of Equation (14) to yield the complex eigenfrequencies as a function of the parameters requires the use of a computer to arrive at useful solutions. The algorithm is a two dimensional Newton-Raphson iteration method, in which the complex frequency is considered as two independent variables. The computation proceeds as follows: the parameter values and the complex frequency is initially assumed and the wavenumbers computed. The complex boundary conditions determinantal function (the left hand side of Equation (14))is then evaluated. For eigenfrequencies, this function is identically zero, but in general it is not. The real and imaginary parts of the frequency are incremented and the four partial derivatives computed. From these a new complex frequency is determined and the process repeated until a convergence test is satisfied or a preset number of iterations exceeded and that particular computation terminated. Once a convergence has been achieved, a parameter (usually the normalized length) is incremented, the starting value for the next computation automatically computed using an extrapolation formula, and the process continued until a branch of an eigenfrequency curve is completed or a non-convergence occurs.

Transient Behavior

While a complete knowledge of the eigenmodes is sufficient to determine the dynamical behavior of the system, it does not leave one

with a very clear physical picture of the transient behavior to some arbitrary initial disturbance. To provide this picture the original equations can be programmed using the method of characteristics.[24] The boundary conditions are that each jet enter the interaction region unexcited. Jet 1 (traveling to the right) is given an initial disturbance; jet 2 is initially unexcited. The resulting transient is shown in Fig. 13 for two values of the electric field very close to but on either side of the point of impending instability, marked points A and B in Fig. 11.

The initial disturbance grows while it propagates downstream, illustrating the convectively unstable character of the jets. As it propagates it exerts a traction on jet 2 pulling it away from equilibrium (T = 5). At T = 10, the initial disturbance has been swept out of the interaction region and the shape of the fundamental symmetric mode begins to appear. As time progresses, this mode grows and the higher modes disappear. Since point A is close to the point of impending instability, the growth rate of the instability is quite slow.

In Fig. 13(b) the same conditions are used except the electric field is reduced to just below the instability point. Now, however, the amplitude growth of jet 1 cannot produce sufficient traction on the returning jet to sustain the disturbance, and the amplitudes decay slowly in time.

If sufficient electric field is applied to the system so that the A2 mode is also unstable and the same conditions applied, it is found that after a short transient in which the initial transient is swept downstream, the system settles down to a combination of the two unstable modes, but since the S1 mode is more unstable, this mode ultimately dominates.

Magnetic Field Coupling

As previously mentioned, the magnetic field and electric field coupled systems are closely analogous, the principle difference being that the self coupling term is stabilizing for magnetic field systems, while being destabilizing for electric field systems. One might expect therefore that the magnetic field coupled counter-streaming jets to be less unstable, which is verified in Fig. 14.

As in the case of electric field coupling: (1) for small magnetic field, all modes are decay modes with $\omega_i \to \infty$ as $L\omega_h/V_o \to 0$, (2) for $L\omega_h/V_o \to \infty$ the unstable modes approach the saddle point frequency and (3) the lowest S and A modes are static modes. In contrast, however, all modes exhibit instability and the instability is in all cases static. As in electric field coupling the fundamental modes dominate the dynamics although now both the symmetric and antisymmetric modes must be considered.

At the point of impending instability $\omega = 0$ and an analysis similar to the derivation of Equation (15) yields

$$\tan\left\{\sqrt{\frac{\eta+1}{2}}\,\frac{\omega_h L}{\sqrt{V_o^2-V_t^2}}\right\}\tan\left\{\sqrt{\frac{\eta-1}{2}}\,\frac{\omega_h L}{\sqrt{V_o^2-V_t^2}}\right\}+\sqrt{\frac{\eta-1}{\eta+1}}\,\sqrt{\frac{\eta+1}{\eta-1}} = 0 \quad \binom{S}{A} \qquad (17)$$

As seen in Fig. 15 the transverse boundaries have an important effect in determining whether the S or A mode will be the first to go unstable. Also the effect of the transverse plate spacing is opposite to the electric field case. Since the magnetic field is inherently stabilizing, bringing the plates close to the jets will impede the destabilizing effect of the flow.

The eigenfunctions at the point of impending instability are given by:

$$\hat{\xi}_{1(x)} = \xi_o \left\{ \frac{\sin\beta_1 x}{\sin\beta_1 L} \pm \frac{\cos\beta_2 x}{\cos\beta_2 L} \right\} \qquad S$$

$$\hat{\xi}_{1(x)} = \xi_o \left\{ \frac{\cos\beta_1 x}{\cos\beta_1 L} \pm \frac{\sin\beta_2 x}{\sin\beta_2 L} \right\} \qquad A \qquad (18)$$

where $\beta_{1\atop 2} = \frac{\omega_h}{\sqrt{V_o^2 - V_t^2}} \sqrt{\frac{\eta \mp 1}{2}}$

The trajectories are nearly those shown in Fig. 16 for $L\omega_h/V_o = 4$, where the lowest three modes are plotted for two instants of time, showing the dynamical behavior. The magnetic field eigenfunctions are much more wavelike that those for the electric case.

The transient behavior of the magnetic field coupled system, for conditions similar to those described above for the electric field case, is carried out in reference (18) for points C and D in Fig. 15. The results are in agreement with Eqs. (17) and (18).

An Electrohydrodynamic Experiment

In order to verify at least some of the results of the previous sections, an experiment consisting of two counterstreaming water jets stressed by a transverse electric field was constructed. The length between nozzles and the transverse spacings were carefully kept the same as in the two spring calibration experiment. The jet and spring diameters were also the same.

Because the plates and jets were non-planar, the relative polarity of the electric field in the field regions was important. This was because a jet is influenced by the non-adjacent plate. In the experiments described, the voltage of the elements was of alternate polarity. This minimized the effect of the non-adjacent plate and secondly allowed the use of a single power supply.

In order to produce a suitable jet of sufficient length it was necessary to damp out all sources of noise which would excite the natural sausage (m = 0) mode of instability. Bassett[25] and Melcher[19] have shown that a transverse electric field increases the spatial growth rate of this mode and effectively shortens the useful length of the jet. As a result considerable care was necessary to produce a jet 80 cm long before breakup with the electric field at approximately the breakdown value for air. To help achieve this glycerine was added to increase the viscosity to a sufficient level to damp out the sausage mode without affecting the principle (m = 1) mode. This was practical since the principle mode wavelengths were long, while the sausage mode wavelengths were on the order of about 1 cm.

The experiment consisted in measuring the decay rate vs. voltage for the lowest mode of the system. A small DC voltage was impressed on the normally grounded plate to deflect the jets, with a large DC voltage on. With the jets deflected, the plate was grounded and the decay transient recorded. The results are shown in Fig. 17 and the theoretical results are seen to be in agreement with the experiment.

For a low applied voltage, the decay transient is quite rapid and a bit difficult to interpret. In order to measure the fundamental mode unambiguously it is assumed that all higher modes have damped before the

usable portion of the decay curve has been reached. This was near the end of the transient but before the transient became noise limited. As the voltage was increased, the decay curves were more nearly exponential, but near the point of instability the jets became quite noisy. Because of the jet break up at the highest voltages, the equipotential model was no longer valid and the experimental data was not in agreement with the theoretical value.

It should be noted that the jet velocity was approximately 30 times the capillary velocity, so that the effect of surface tension on these measurements was completely negligible.

VI Conclusions

The basic electrodydrodynamic and magnetohydrodynamic surface waves for an incompressible fluid have been classified and investigated by Melcher.[19] In studies of single streams, the free charge, electric field coupled and free current, magnetic field coupled models have been extended to include the effect of convection. Until now there has been no work reported in the literature concerning the two-stream systems. Since long waves are the most important the procedure adopted is to consider only the principal transverse modes and to investigate the longitudinal modes in detail. The resulting equations of motion for the systems considered here (kink modes of the streams), consist of two coupled hyperbolic partial differential equations. This is fortunate, since then the method of characterisitics may be used to provide the answer as to how to specify boundary conditions which do not violate causality. For example, it is unphysical to specify a downstream boundary condition on a supercapillary jet, whether field coupled to another jet or not. This concept is often overlooked in the literature.

For the more general problem when the principal mode results in the equations of motion not being of the pure hyperholic type (for example the long wave sausage mode of a single jet) the question of specifying boundary conditions consistent with causality must be reexamined. To the author's knowledge, this problem has not been investigated.

For the problem of two field coupled streams considered in this paper, it is shown that there are four flow configurations which are basically different.

For the classes of flow in which boundary conditions exist at more then one point in space (Classes I, III, and IV), an infinite set of eigenmodes exist and the eigenfrequencies (complex in general) and time dependant eigenfuctions can be computed to given the detailed structure of the system dynamics. When causal boundary conditions exist at only one point in space, as in Class II flow, no eigenmodes exist and hence no absolute instabilities are possible.

The dynamics of two finite length field coupled streams has been discussed and compared (1) to the infinite length system (2) one flow regime with another (3) with respect to the type of field coupling (4) to their single stream counter parts. While some of the properties of the finite length system can be inferred from the infinite length system (dispersion relation and Bers-Briggs criterion), yet important effects exist which require the boundaries for explanation, such as the overstabilities for the counter streaming electric field coupled system.

There exists a close analogy between magnetic field coupled conducting streams and electrostatic oscillations of electron beams.

The equation of motion for two interpenetrating electron beams is that given by equation (1) for the magnetic field coupled case if the surface tension term is suppressed and $\eta = 1$.

Since electron beams contain no effective "surface tension," Class I flow does not exist and costreaming beams exhibit only the convectively unstable regime. The Class III flow, counterstreaming beams, exhibits eigenfrequency plots similar to those shown in Fig. 15, i.e., all modes, both symmetric and antisymmetric, exhibit purely static instability. This model is currently being extended to explain the overstabilities observed by Kofoid in his experiments with counterstreaming electron beams in the presence of a background plasma.

Acknowledgements

I would like to express my sincere gratitude to Professor James R. Melcher of M.I.T. for his guidance and help throughout this work. The numerical work was performed at the M.I.T. Computation Center. This work was supported by the NASA under grant NsG-368.

Figure Captions

Figure 1. Two highly conducting fluid streams in relative motion are coupled by means of an applied electric or magnetic field.

Figure 2. Dispersion curves, assuming solutions of the form exp $j(\omega t - kx)$ for the long wave model ($\lambda >> a$) of the system of Figure 1. Complex ω has been plotted for real k. Both streams have subcapillary fluid velocity (class I flow), with (a) and (b) electric field coupled and (c) and (d) magnetic field coupled. Curves (a) and (c), with the mutual coupling ignored, have been included for comparison.

Figure 3. Stability curves for electric field coupling for the conditions of Figure 2. Complex k is plotted for fixed ω_r as ω_i is increased from $-\infty$ to o. Two saddle points are apparent for the "2" curves, indicating static-type ($\omega_i = o$) absolute instabilities.

Figure 4. Frequency dependance on applied electric field for the fundamental symmetric and antisymmetric modes for two springs stresses by a transverse electric field. The dashed curve is based on Eq. (5).

Figure 5. Dispersion curves for co-streaming, supercapillary jets (class II), electric field coupling, are shown for two flow conditions. Complex ω is plotted for real k. The system exhibits convective instability for both flow conditions. The mutual coupling is suppressed in (a) and (c).

Figure Captions Continued

Figure 6. Dispersion curves for class II flow, magnetic field coupling, for conditions similar to Figure 5. For $|V_{o1} - V_{o2}| < 2V_t$, as in (b), only propagating waves are present, whereas, the system is convectively unstable if $|V_{o1} - V_{o2}| > 2V_t$ (Figure 6 (d).)

Figure 7. Dispersion curves for supercapillary, counter-streaming flow (Class III). Electric field coupling is shown in (a) and (b), magnetic field coupling in (c) and (d). Complex ω is plotted for real k and the mutual coupling is suppressed in (a) and (c).

Figure 8. Class III stability curves: (a) electric field coupling produces a strong static instability (curves 1) and a weak overstability (curves 3 and 4). (b) magnetic field coupling produces an overstability (curves 1 and 2).

Figure 9. Sketch of symmetry modes for similar counter-streaming jets.

Figure 10. Complex eigenfrequencies vs. normalized length for similar electric field coupled counter-streaming jets. The fundamental symmetric mode (S1) exhibits static instability $L\omega_e/V_o > 1.1$. Higher modes (A2, S3, A4, etc.) exhibit overstability and then static instability as $L\omega_e/V_o$ is increased. ω_r is symmetric about the abscissa and only one branch is shown.

Figured Captions Continued

Figure 11. Effect of transverse geometry on the normalized length for the system of Figure 10 at the point of impending instability.

Figure 12. Time dependent eigenfunctions for the three lowest symmetric and antisymmetric modes for the conditions of Figure 10. $L\omega_e/V_o = 3$

Figure 13. Transient behavior of two similar counter-streaming electric field coupled jets. The lower jet, traveling to the right, is given an initial displacement. Stable components of this excitation propagate away, leaving only the fundamental symmetric mode which slowly becomes unstable in (a) and slowly decays away in (b). Points A and B are shown in Figure 11.

Figure 14. Complex eigenfrequencies vs. normalized length for similar magnetic field coupled counter-streaming jets. All modes exhibit static instability, the growth rate approaching the saddle point as $L\omega_h/V_o \to \infty$. The real part of the eigenfrequency is symmetric about the abscissa and only one branch is shown.

Figure 15. Effect of transverse geometry on the normalized length at the point of impending instability for the fundamental symmetric and antisymmetric modes. The conditions are the same as in Figure 14.

Figure 16. Time dependent eigenfunctions for the three lowest symmetric and antisymmetric modes corresponding to the eigenfrequencies of Figure 14. $L\omega_h/V_o = 4$

Figure 17. Fundamental symmetric mode decay rate vs. applied voltage for electric field coupled counter streaming jets.

References

1. Helmholtz, H., Wissenchaftliche Abhandlungen, 146-57, J. A. Barth, Leipzig, 1882; translation by Guthrie in Phil. Mag. Ser. 4, 36, 337-46 (1868).

2. Chandrasekhar, S., Hydrodynamic and Hydromagnetic Stability, Oxford at the Clarendon Press, 1961.

3. Betchov, R. and Szewczyk, A., Phys. Fluids 6, 1391 (1963).

4. Fejer, J. A., Phys. Fluids 7, 499 (1964).

5. Michael, D. H., Proc. Cambridge Phil. Soc. 51, 528 (1955).

6. Northrop, T. G., Phys. Rev. 103, 1150 (1956).

7. Alterman, F., Phys. Fluids 4, 1207 (1961).

8. Sen, A. K., Phys. Fluids, 6, 8, 1154 (August, 1963).

9. Lyon, J. F., S. M. Thesis, E.E. Dept., M.I.T., Cambridge, Mass. (1962).

10. Talwar, S. P., Phys. Fluids 8, 1295 (1965).

11. D'Angelo, N. and V. Goeler, S., Phys. Fluids 9, 309 (1966).

12. Tosema, S. and Hirota, R., J. Appl. Phys. 34, 2993 (1963).

13. Getty, W. D. and Smullin, L. D., J. Appl. Phys. 34, 3421 (1963).

14. Kofoid, M. J., Boeing Scientific Research Lab., December, 1961.

15. Gerwin, R. and Nelson, D. J., Boeing Scientific Research Lab., Plasma Physics, March, 1964.

16. Louisell, W. H., Coupled Mode and Parametric Electronics, John Wiley and Sons, 1960.

17. Crowley, J. M., Phys. Fluids 8, 1668 (1965).

18. Ketterer, F. D., Ph.D. Thesis, E.E. Dept, M.I.T. (Sept. 1965)

19. Melcher, J. R., Field Coupled Surface Waves, M.I.T. Press (1963). Included in this text is a discussion of the equations governing electrohydrodynamic and magnetohydrodynamic surface phenomena and detailed consideration of the stability of a highly conducting field coupled fluid stream. The antiduality of electric and magnetic coupled systems is exploited. (See p.56)

20. Courant, R. and Friedrichs. K., Supersonic Flow and Shock Waves, Vol. 1, Interscience Publishers, 1948.

21. Bers, A. and Briggs, R., QPR No. 71, RLE, M.I.T., October 16, 1963, pp. 122-130.

22. Briggs, R., Electron Stream Interactions with Plasma, The M.I.T. Press, 1964, Chapter 2.

23. Taylor, G. I., Proc. Royal Soc. A253, 289 (1959).

24. Fox, L., Numerical Solution of Ordinary and Partial Differential Equations, Pergamon Press, 1962.

25. Bassett, A. B., Am. J. of Math. 16, 93 (1894).

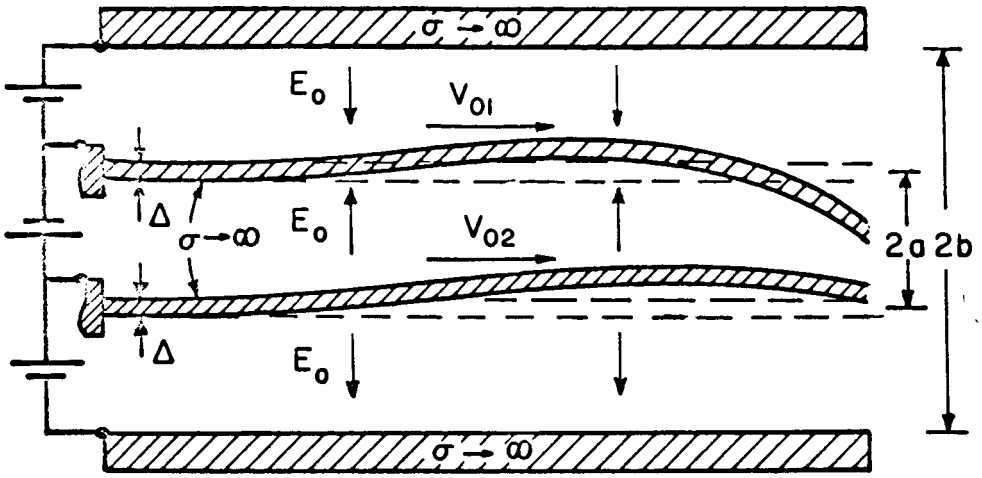

(a) ELECTRIC FIELD COUPLED

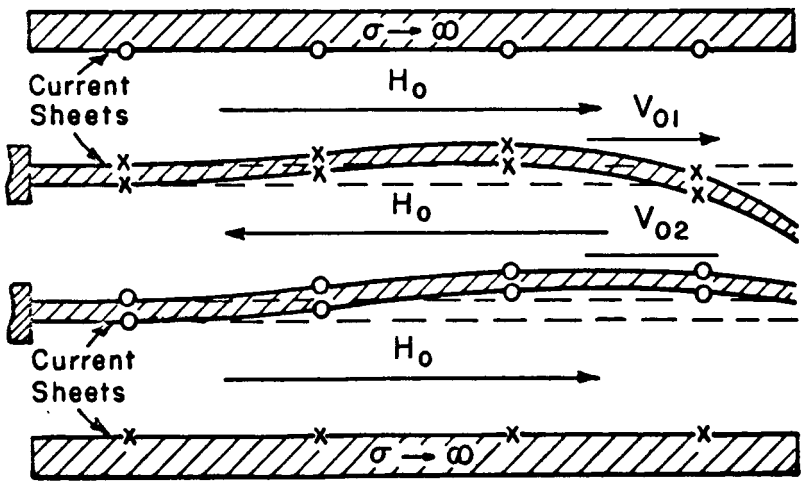

(b) MAGNETIC FIELD COUPLED

Figure 1. Two highly conducting fluid streams in relative motion are coupled by means of an applied electric or magnetic field.

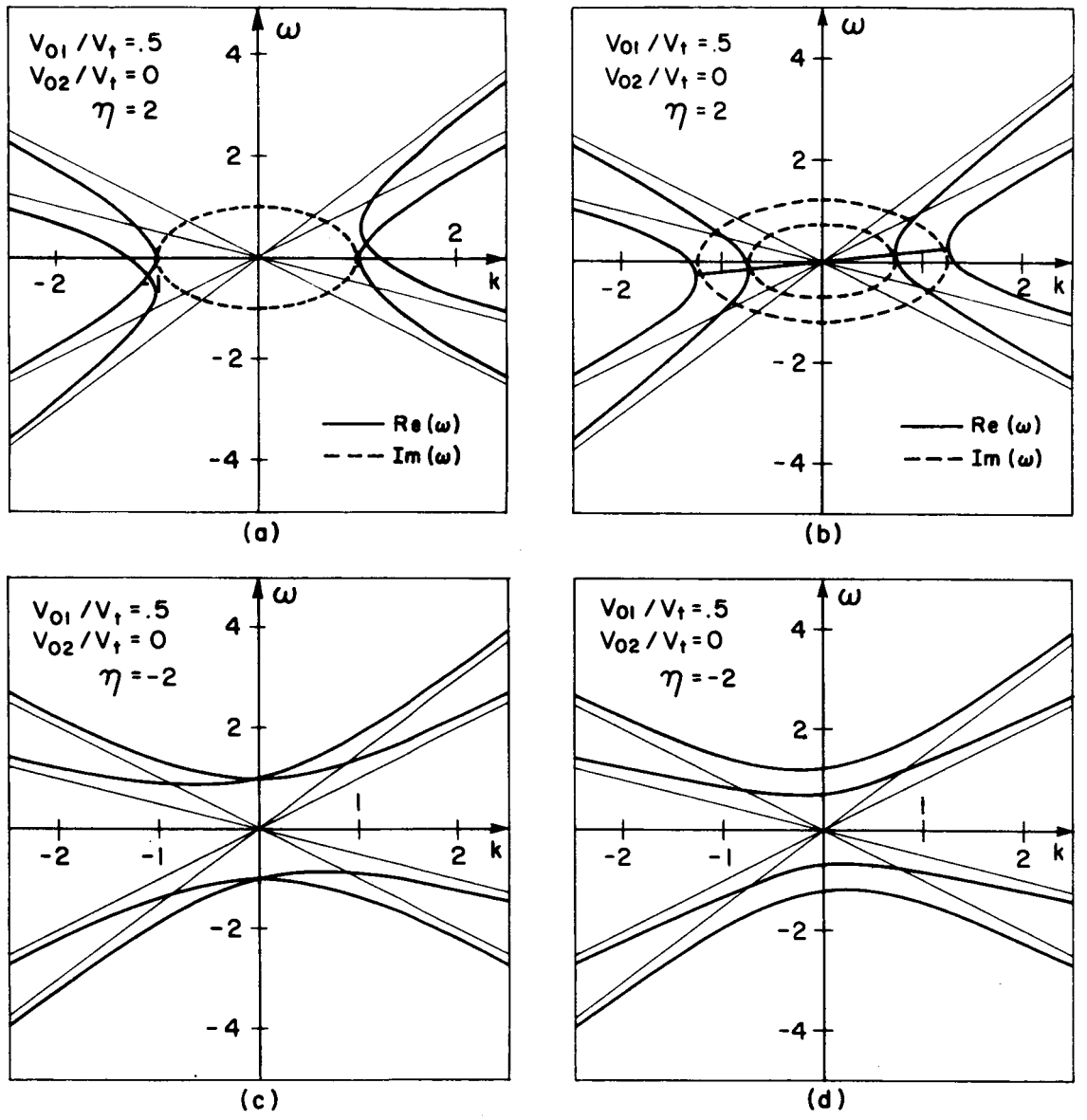

Figure 2. Dispersion curves, assuming solutions of the form exp $j(\omega t - kx)$ for the long wave model ($\lambda >> a$) of the system of Figure 1. Complex ω has been plotted for real k. Both streams have subcapillary fluid velocity (class I flow), with (a) and (b) electric field coupled and (c) and (d) magnetic field coupled. Curves (a) and (c), with the mutual coupling ignored, have been included for comparison.

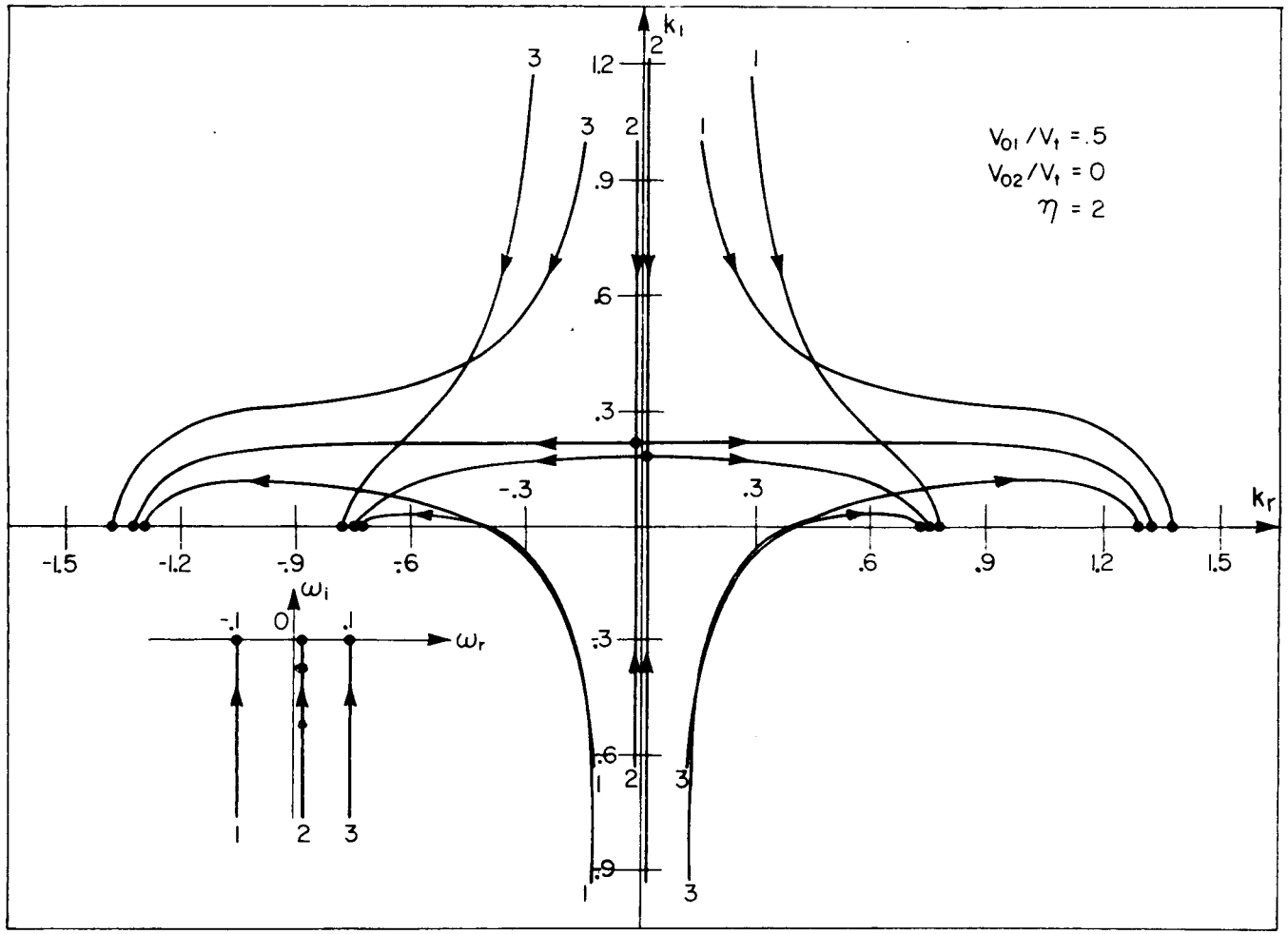

Figure 3. Stability curves for electric field coupling for the conditions of Figure 2. Complex k is plotted for fixed ω_r as ω_i is increased from $-\infty$ to o. Two saddle points are apparent for the "2" curves, indicating static-type (ω_i = o) absolute instabilities.

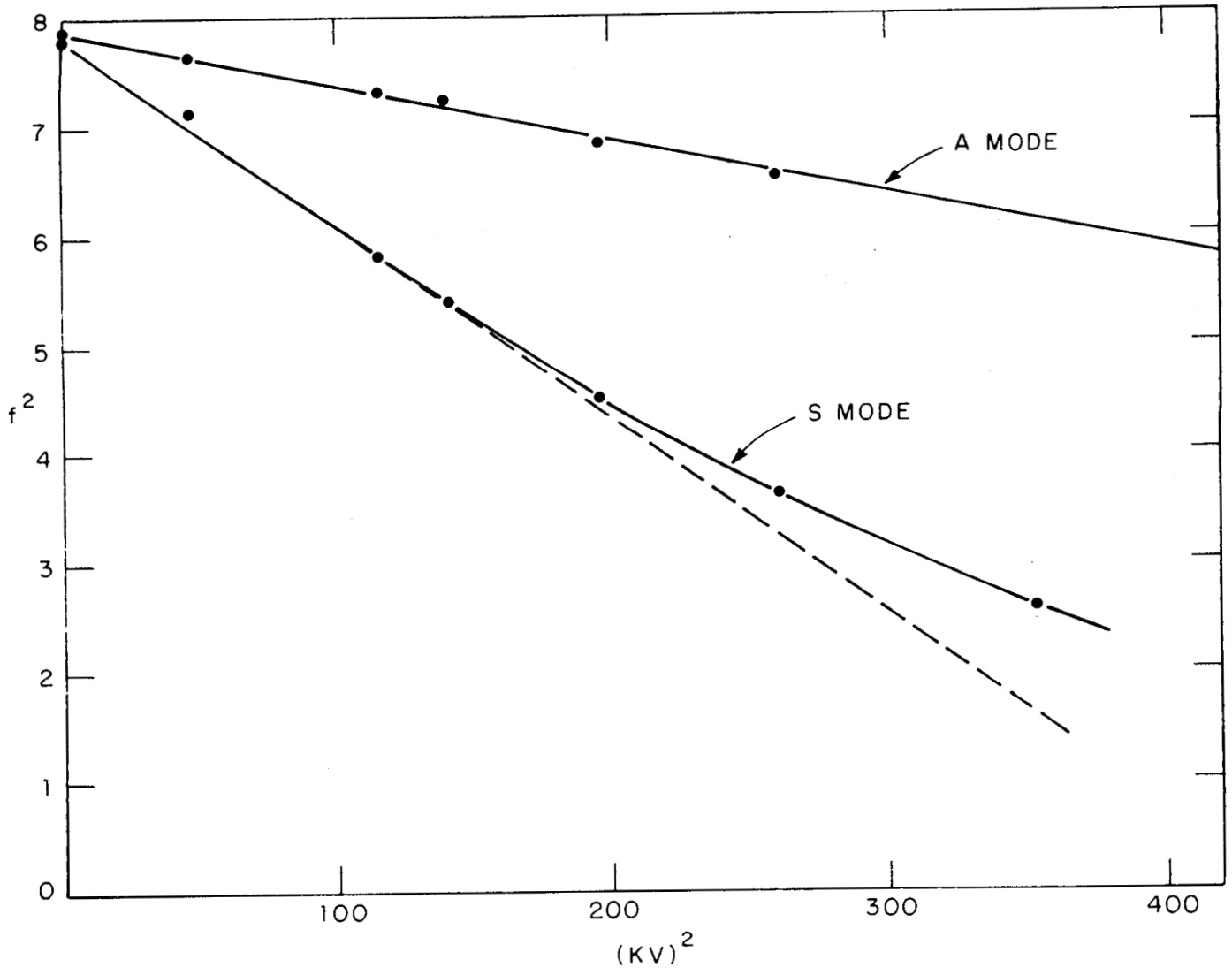

Figure 4. Frequency dependance on applied electric field for the fundamental symmetric and antisymmetric modes for two springs stresses by a transverse electric field. The dashed curve is based on Eq. (5).

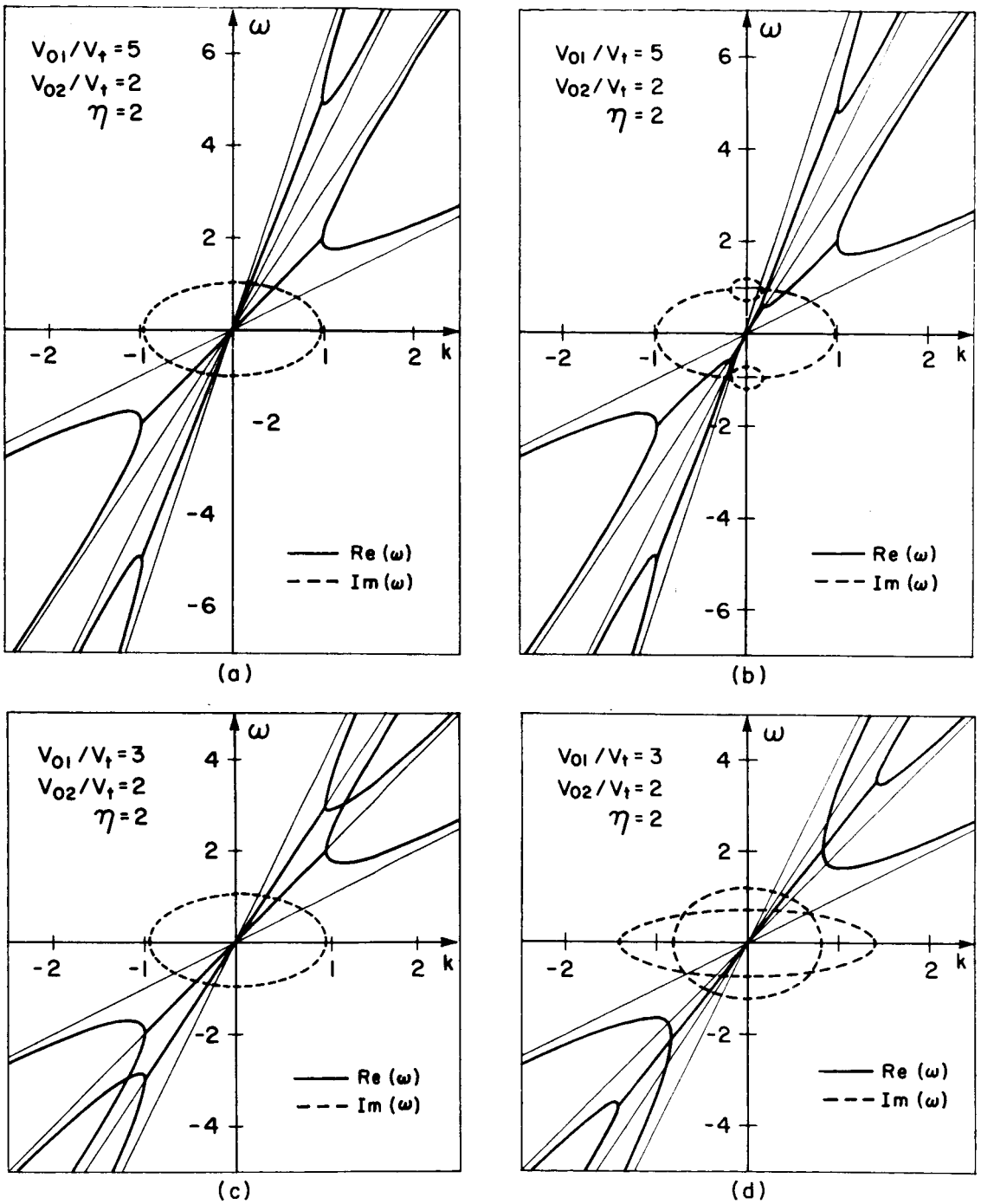

Figure 5. Dispersion curves for co-streaming, supercapillary jets (class II), electric field coupling, are shown for two flow conditions. Complex ω is plotted for real k. The system exhibits convective instability for both flow conditions. The mutual coupling is suppressed in (a) and (c).

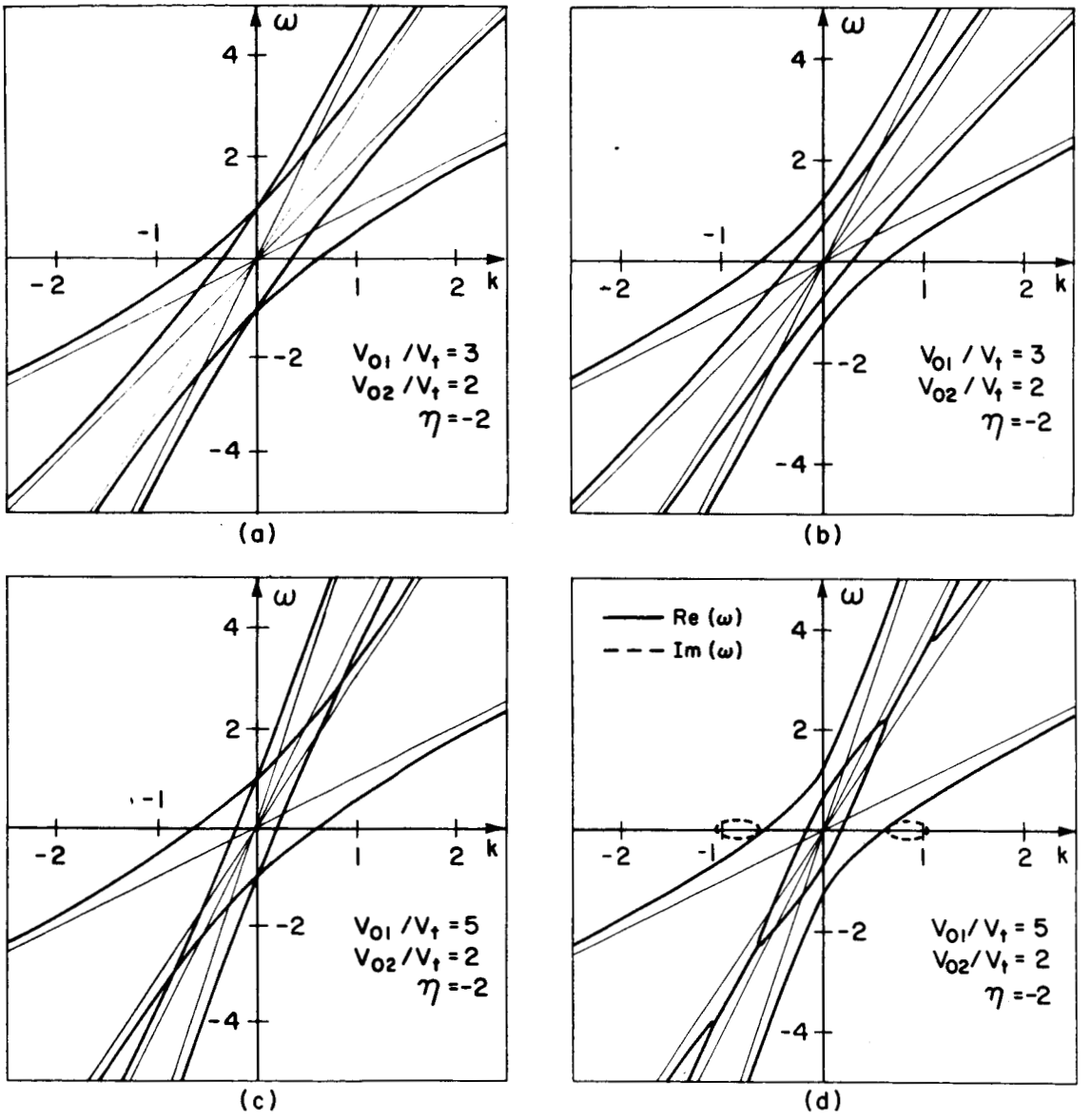

Figure 6. Dispersion curves for class II flow, magnetic field coupling, for conditions similar to Figure 5. For $|V_{o1} - V_{o2}| < 2V_t$, as in (b), only propagating waves are present, whereas, the system is convectively unstable if $|V_{o1} - V_{o2}| > 2V_t$ (Figure 6 (d).)

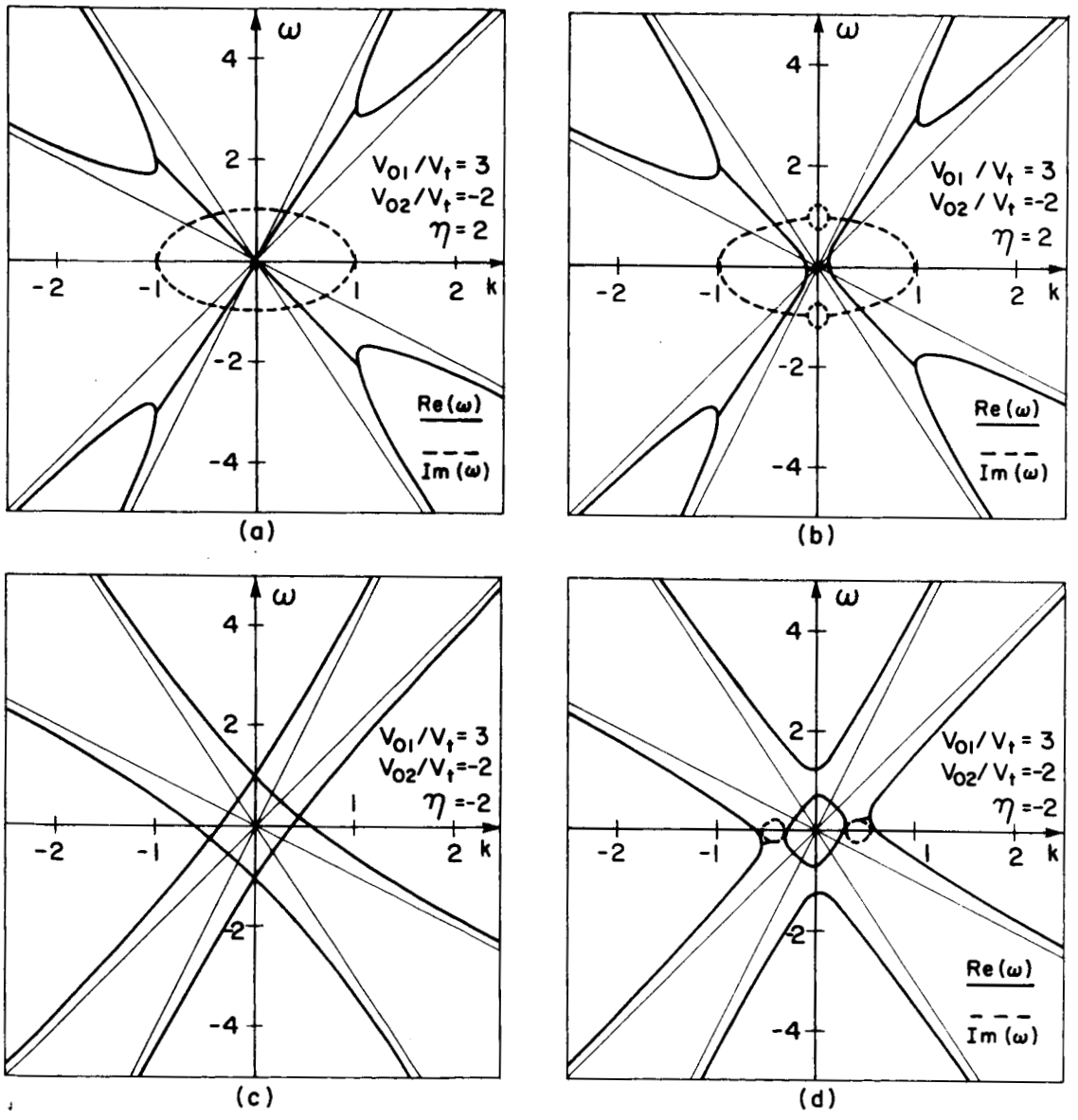

Figure 7. Dispersion curves for supercapillary, counter-streaming flow (Class III). Electric field coupling is shown in (a) and (b), magnetic field coupling in (c) and (d). Complex ω is plotted for real k and the mutual coupling is suppressed in (a) and (c).

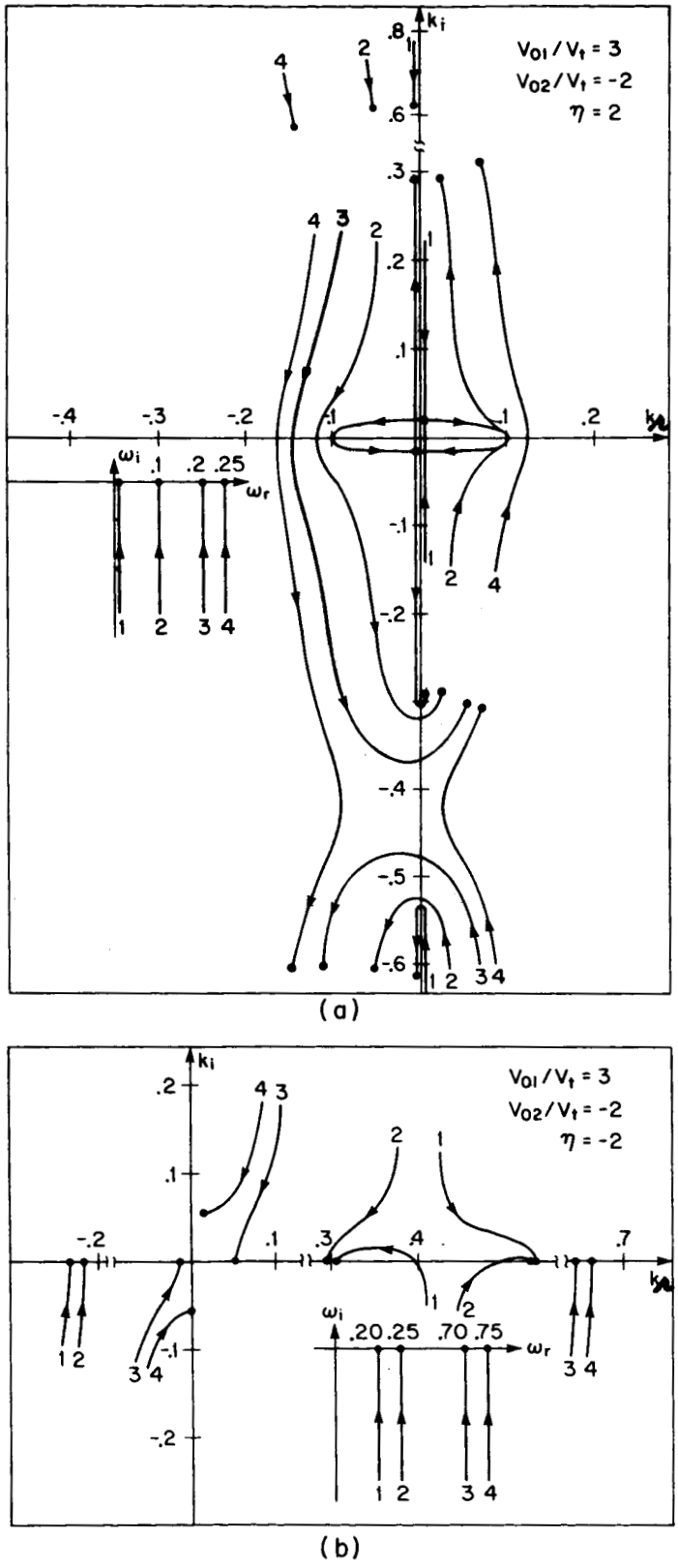

Figure 8. Class III stability curves: (a) electric field coupling produces a strong static instability (curves 1) and a weak overstability (curves 3 and 4). (b) magnetic field coupling produces an overstability (curves 1 and 2).

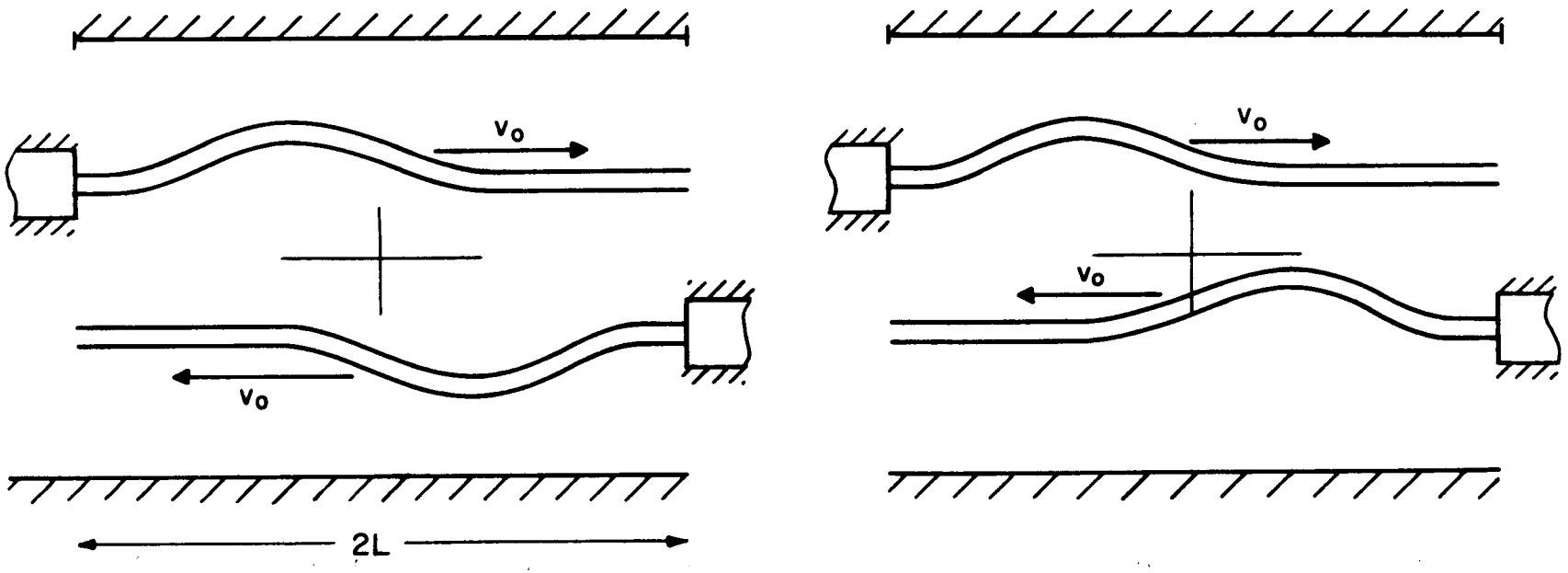

Figure 9. Sketch of symmetry modes for similar counter-streaming jets.

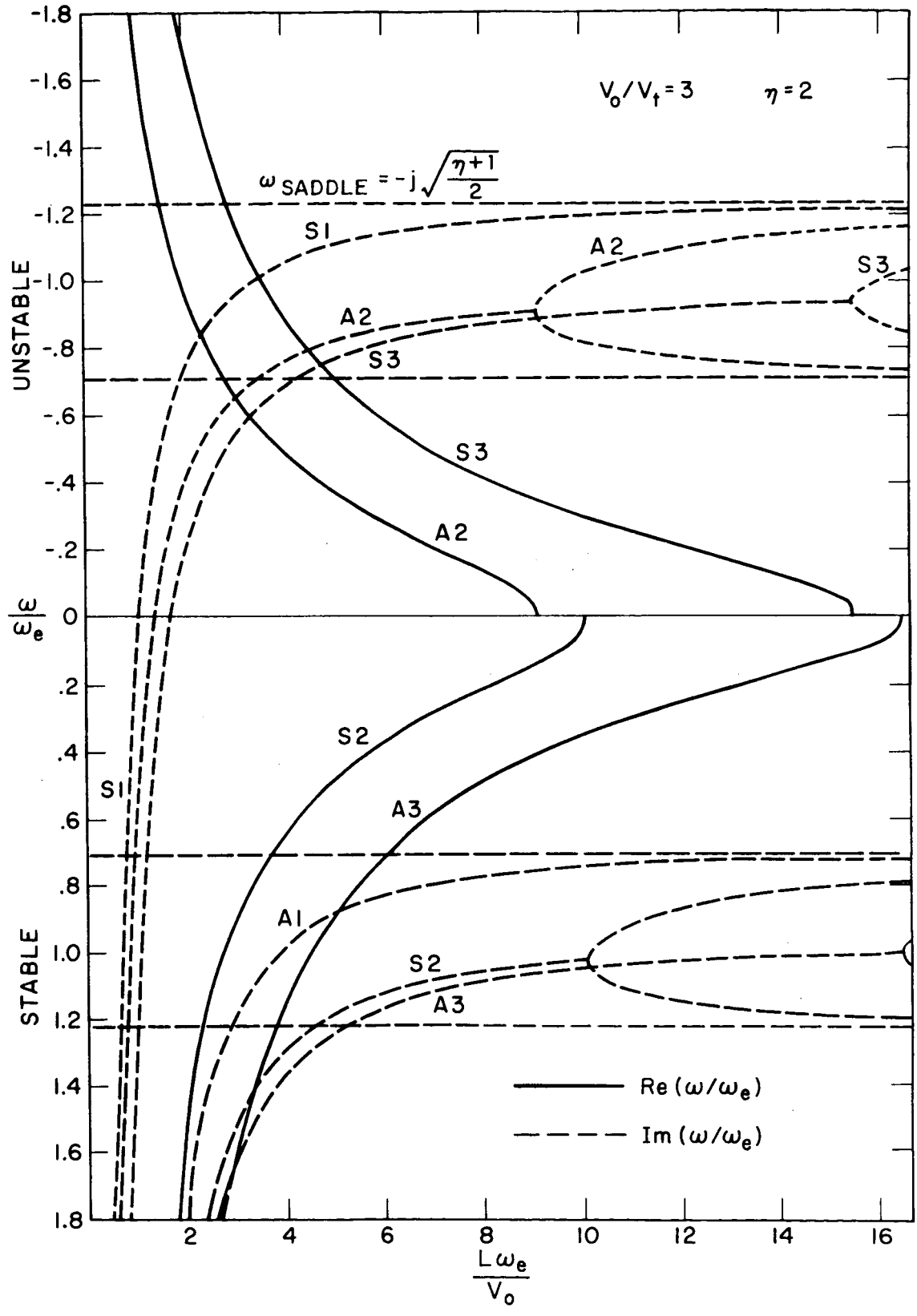

Figure 10. Complex eigenfrequencies vs. normalized length for similar electric field coupled counter-streaming jets. The fundamental symmetric mode (S1) exhibits static instability $L\omega_e/V_o > 1.1$. Higher modes (A2, S3, A4, etc.) exhibit overstability and then static instability as $L\omega_e/V_o$ is increased. ω_r is symmetric about the abscissa and only one branch is shown.

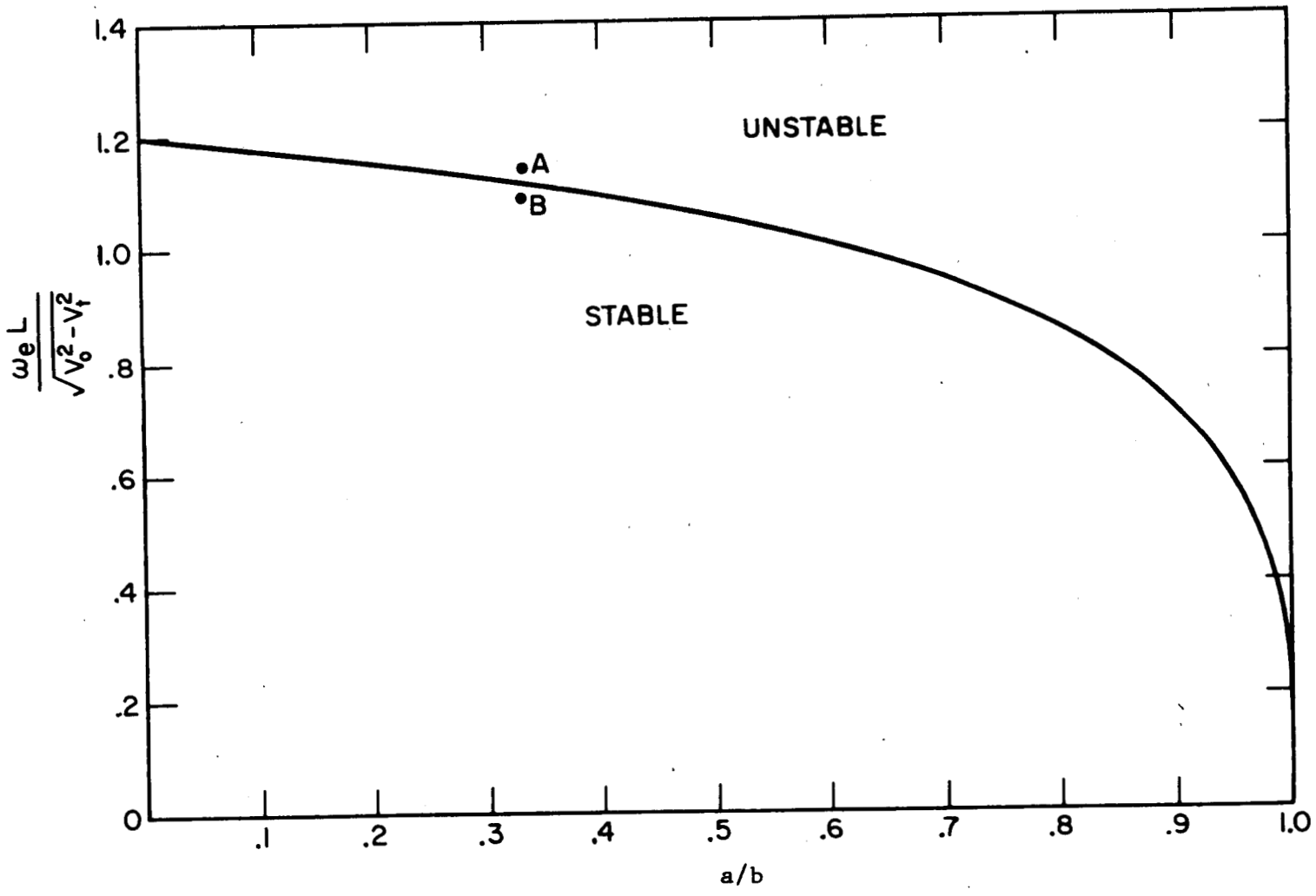

Figure 11. Effect of transverse geometry on the normalized length for the system of Figure 10 at the point of impending instability.

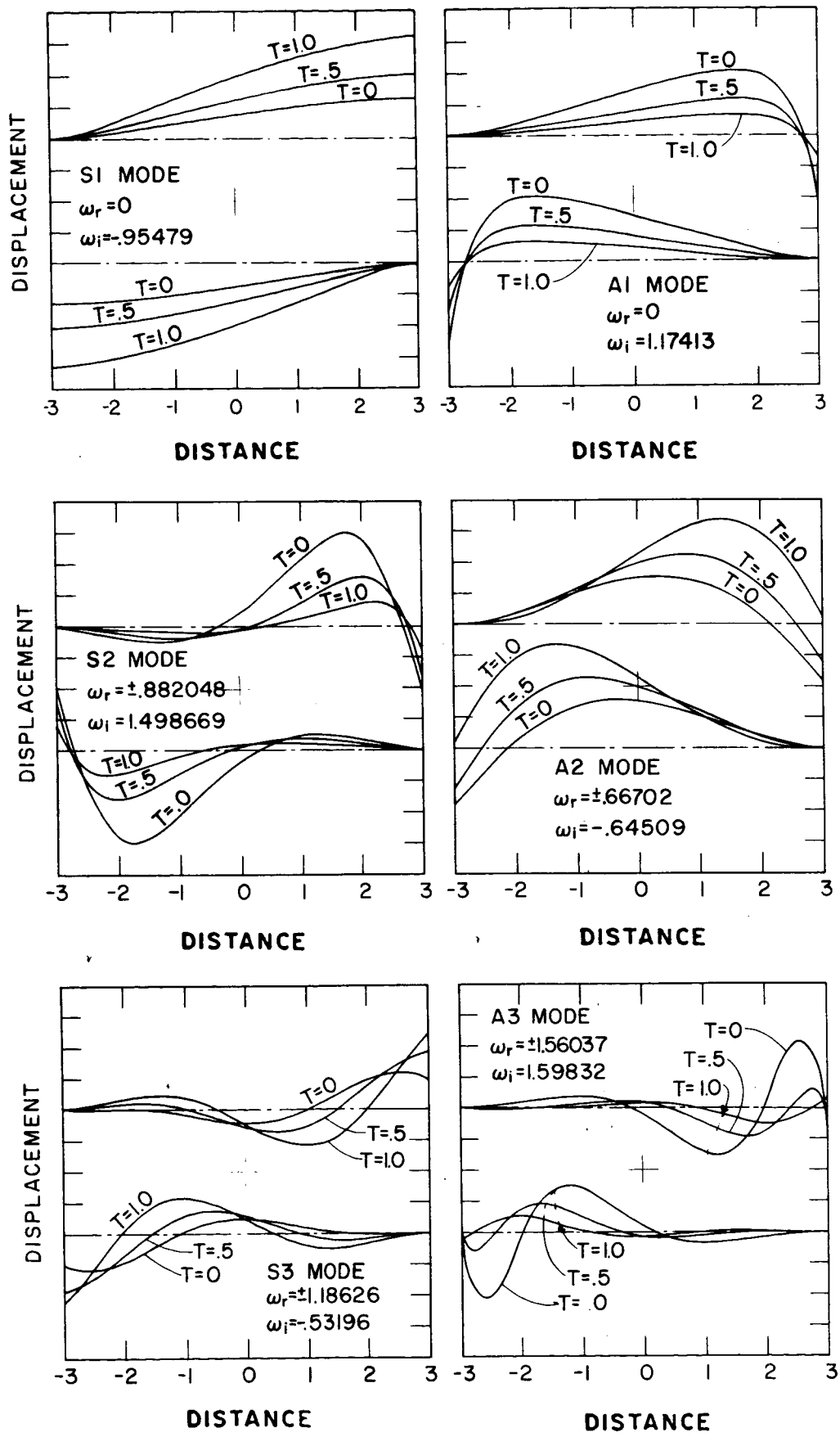

Figure 12. Time dependant eigenfunctions for the three lowest symmetric and antisymmetric modes for the conditions of Figure 10. $I\omega_e/V_o = 3$

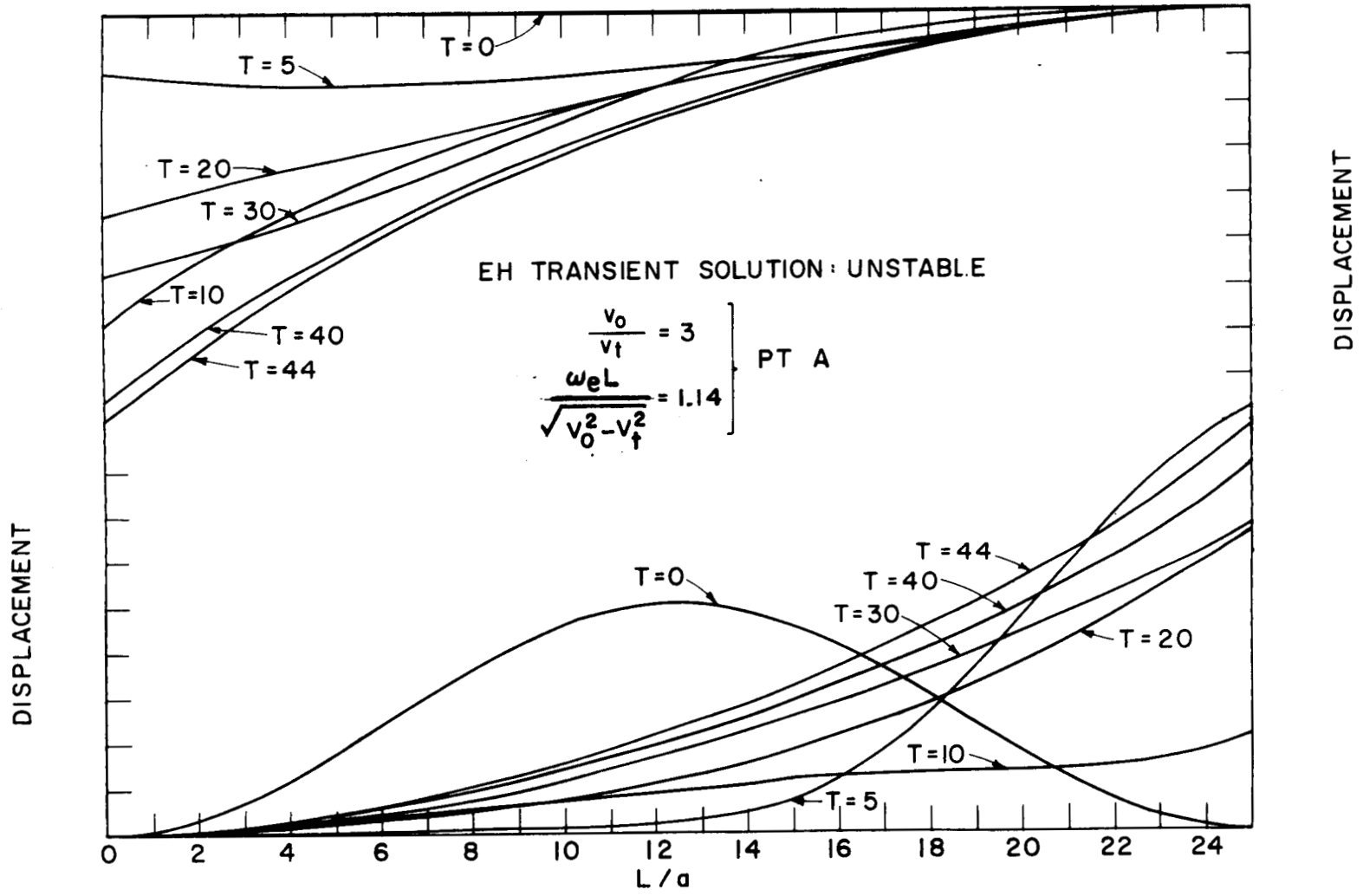

Figure 13. Transient behavior of two similar counter-streaming electric field coupled jets. The lower jet, traveling to the right, is given an initial displacement. Stable components of this excitation propagate away, leaving only the fundamental symmetric mode which slowly becomes unstable in (a) and slowly decays away in (b). Points A and B are shown in Figure 11.

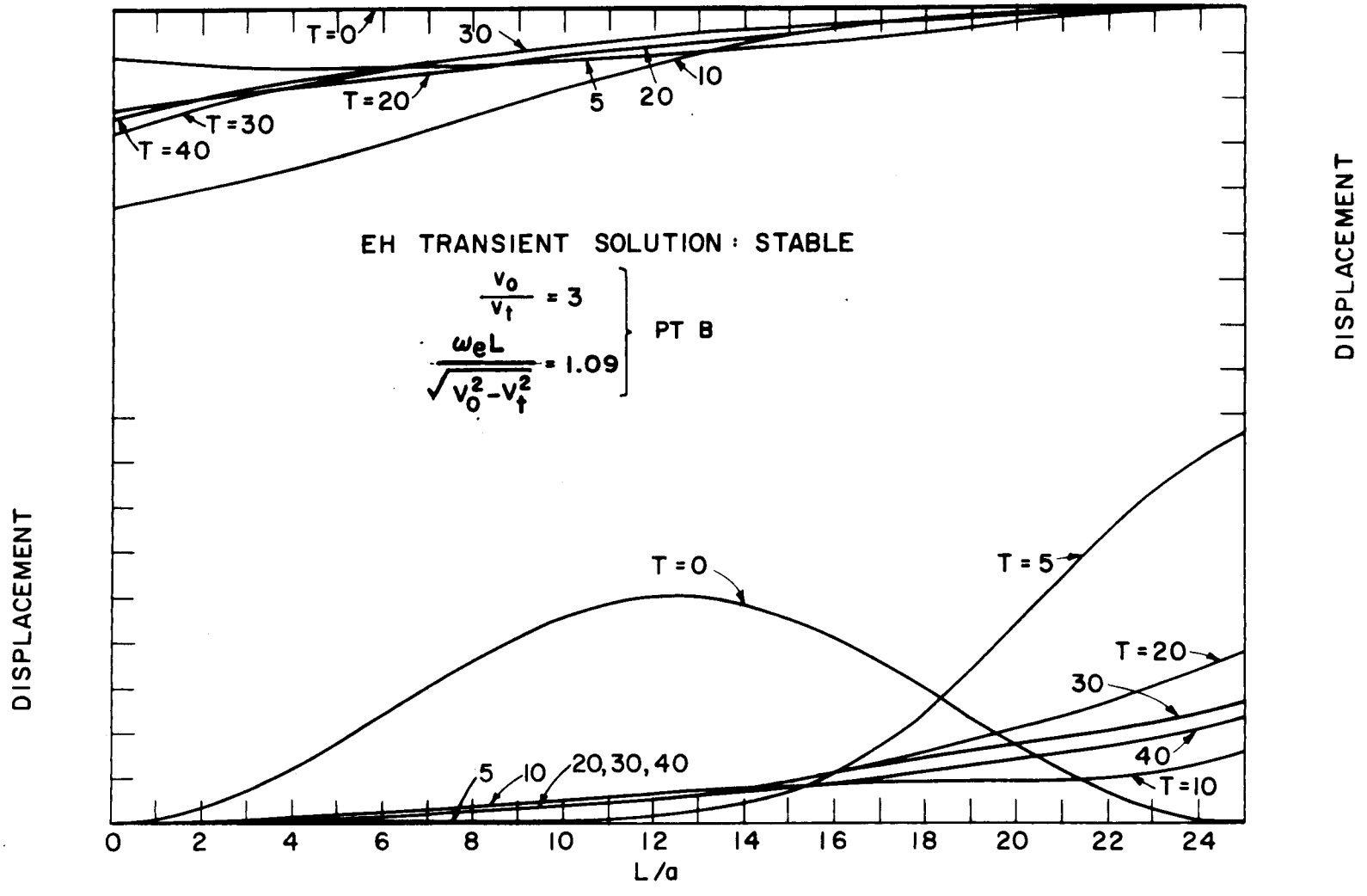
T=0
30
10
T=20
5
20
T=30
T=40
EH TRANSIENT SOLUTION : STABLE
$\frac{V_0}{V_t} = 3$
$\frac{\omega_e L}{\sqrt{V_0^2 - V_t^2}} = 1.09$
PT B
T=0
T=5
T=20
30
40
T=10
5
10
20,30,40
0
2
4
6
8
10
12
14
16
18
20
22
24
L/a
DISPLACEMENT
DISPLACEMENT

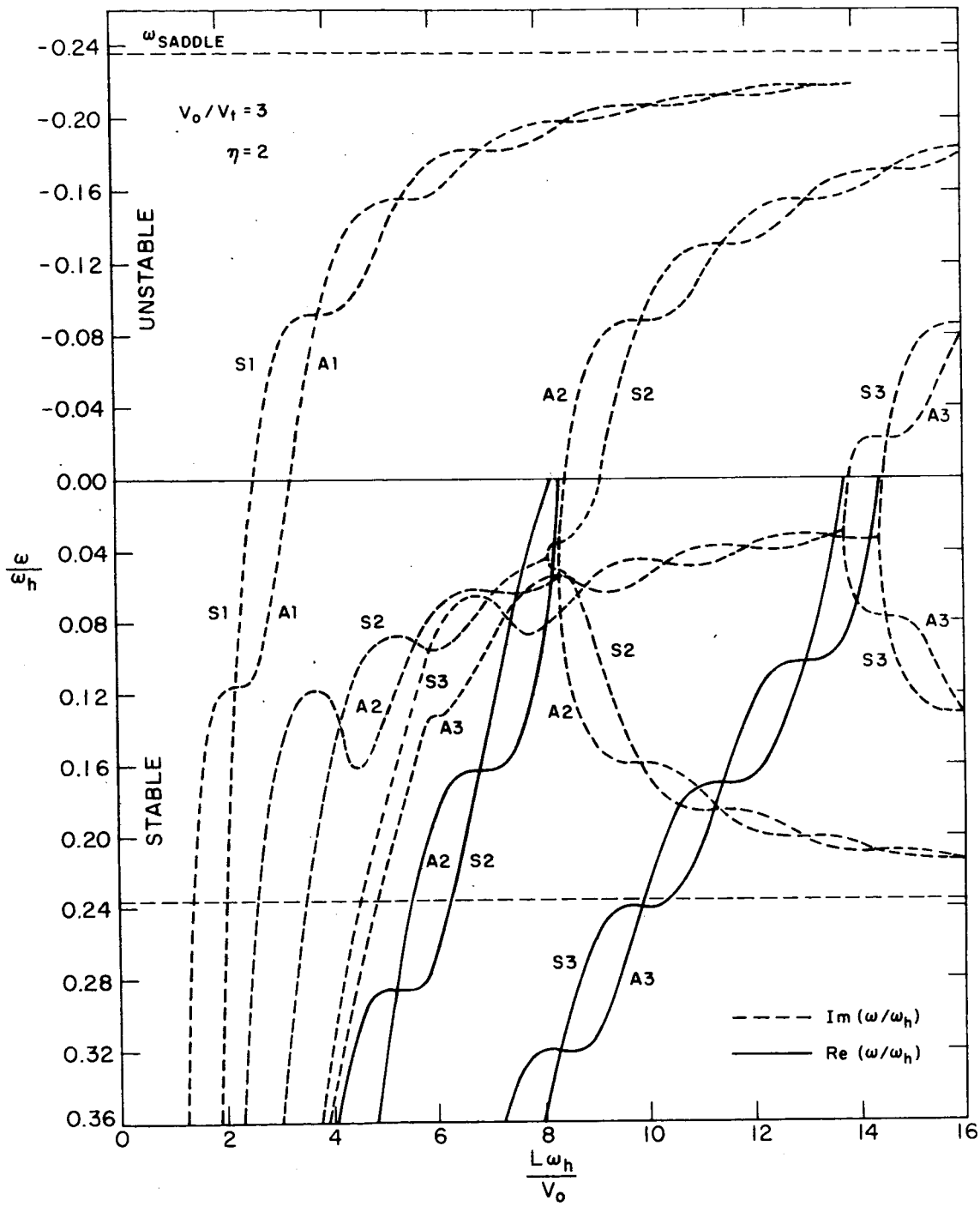

Figure 14. Complex eigenfrequencies vs. normalized length for similar magnetic field coupled counter-streaming jets. All modes exhibit static instability, the growth rate approaching the saddle point as $L\omega_h/V_o \to \infty$. The real part of the eigenfrequency is symmetric about the abscissa and only one branch is shown.

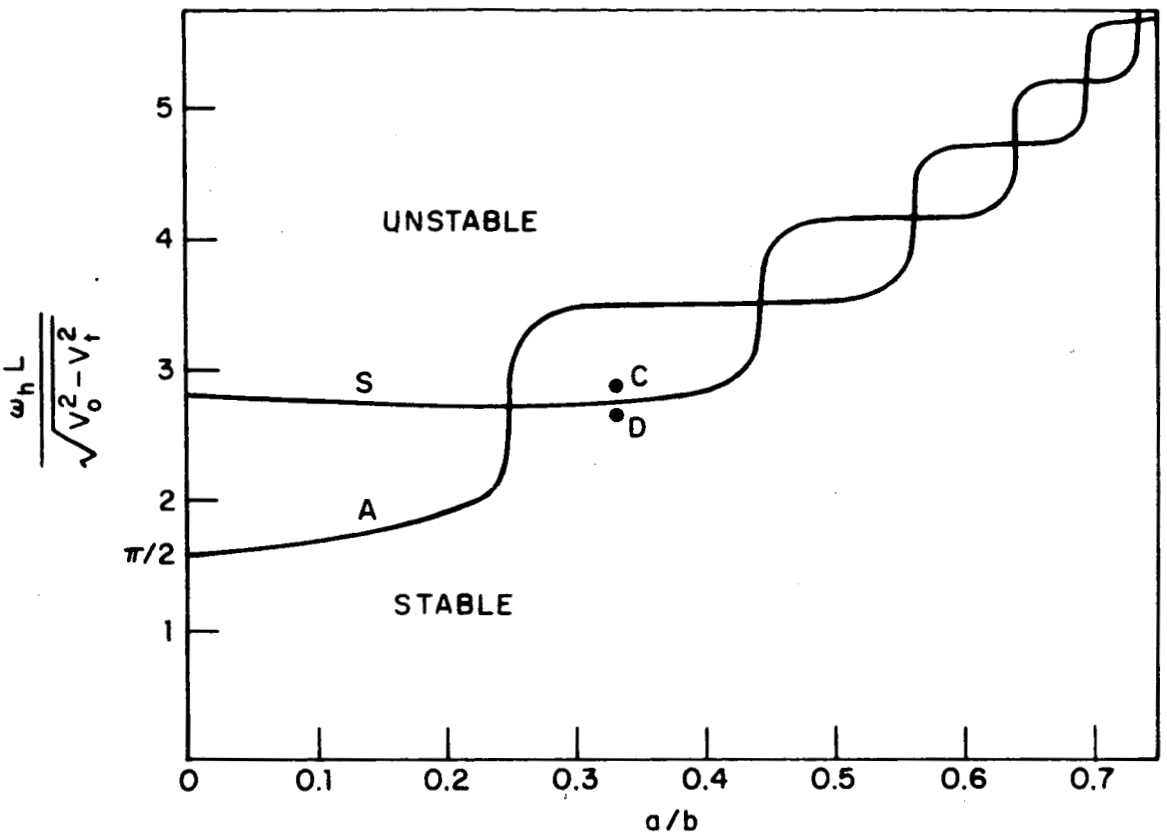

Figure 15. Effect of transverse geometry on the normalized length at the point of impending instability for the fundamental symmetric and antisymmetric modes. The conditions are the same as in Figure 14.

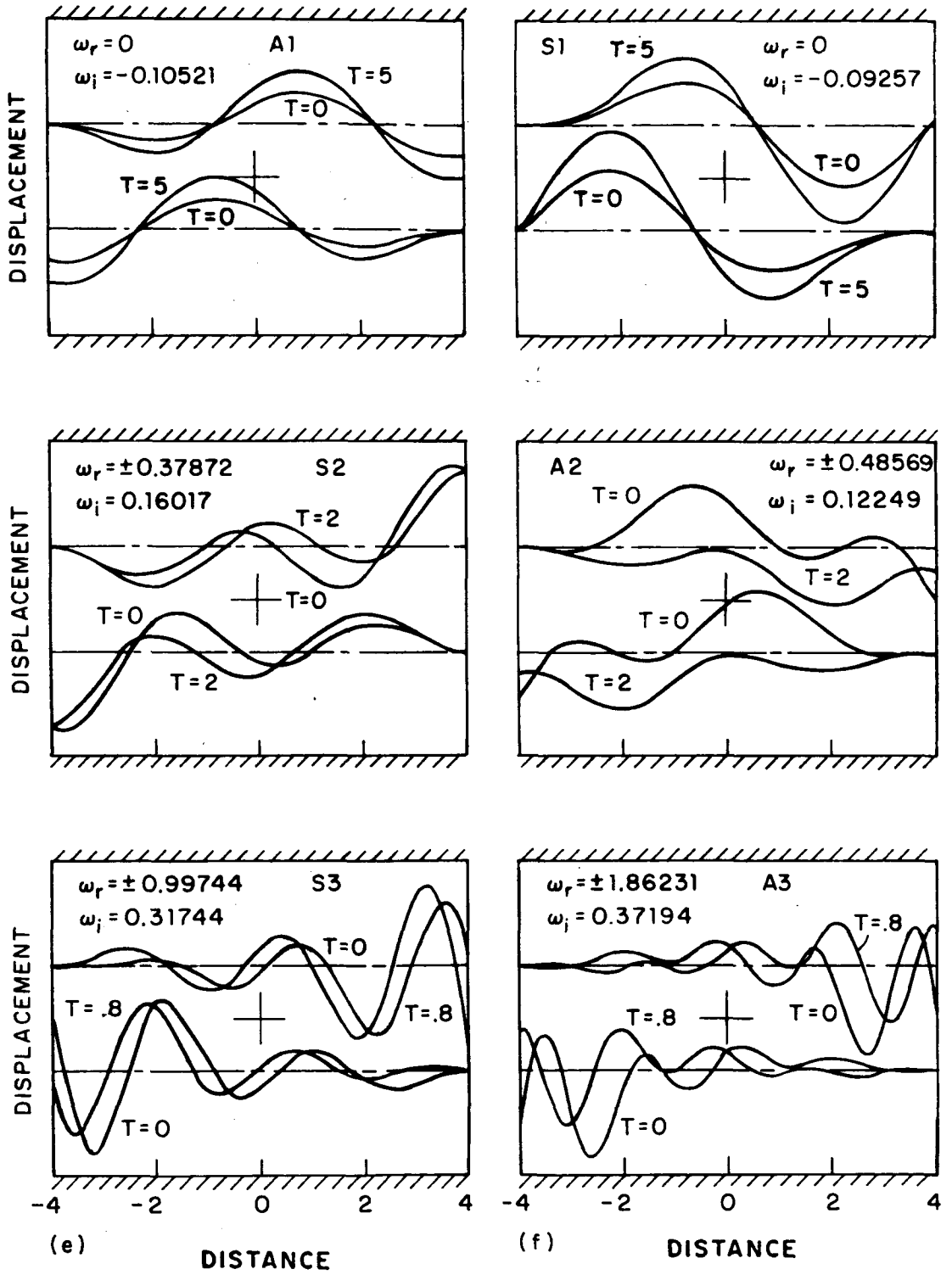

Figure 16. Time dependant eigenfunctions for the three lowest symmetric and antisymmetric modes corresponding to the eigenfrequencies of Figure 14.

$I\omega_h/V_o = 4$

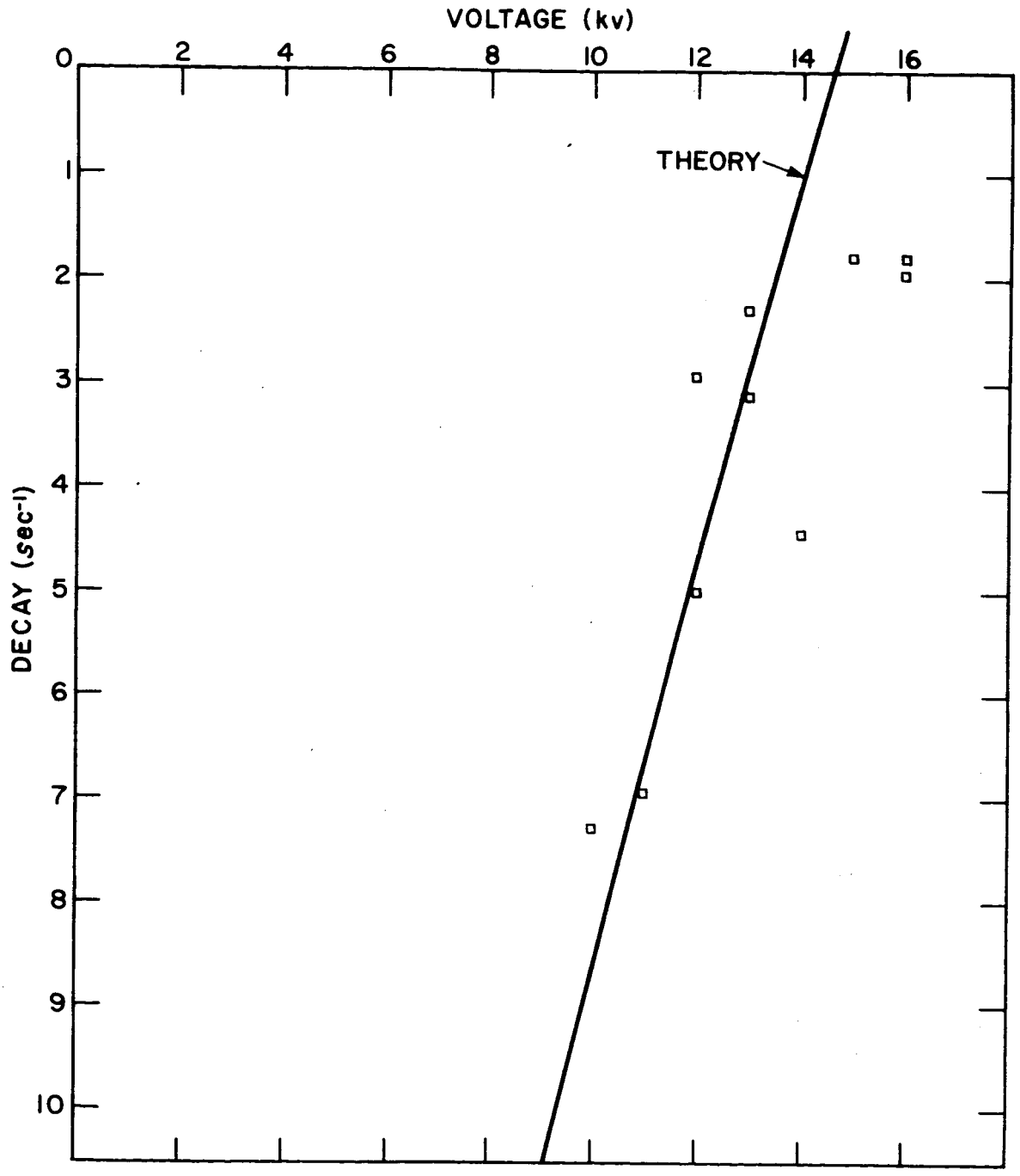

Figure 17. Fundamental symmetric mode decay rate vs. applied voltage for electric field coupled counter streaming jets.